

January 01, 2000

Dispersion of ordered stripe phases in the cuprates

R. S. Markiewicz
Northeastern University

Recommended Citation

Markiewicz, R. S., "Dispersion of ordered stripe phases in the cuprates" (2000). *Physics Faculty Publications*. Paper 135.
<http://hdl.handle.net/2047/d20000746>

This work is available open access, hosted by Northeastern University.

Dispersion of Ordered Stripe Phases in the Cuprates

R.S. Markiewicz

Physics Department and Barnett Institute, Northeastern U., Boston MA 02115

A phase separation model is presented for the stripe phase of the cuprates, which allows the doping dependence of the photoemission spectra to be calculated. The idealized limit of a well-ordered array of magnetic and charged stripes is analyzed, including effects of long-range Coulomb repulsion. Remarkably, down to the limit of two-cell wide stripes, the dispersion can be interpreted as essentially a superposition of the two end-phase dispersions, with superposed minigaps associated with the lattice periodicity. The largest minigap falls near the Fermi level; it can be enhanced by proximity to a (bulk) Van Hove singularity. The calculated spectra are dominated by two features – this charge stripe minigap plus the magnetic stripe Hubbard gap. There is a strong correlation between these two features and the experimental photoemission results of a two-peak dispersion in $\text{La}_{2-x}\text{Sr}_x\text{CuO}_4$, and the peak-dip-hump spectra in $\text{Bi}_2\text{Sr}_2\text{CaCu}_2\text{O}_{8+\delta}$. The differences are suggestive of the role of increasing stripe fluctuations. The 1/8 anomaly is associated with a quantum critical point, here expressed as a percolation-like crossover. A model is proposed for the limiting minority magnetic phase as an isolated two-leg ladder.

I. INTRODUCTION

Evidence for stripe phases in the cuprates continues to grow. Particularly in the $\text{La}_{2-x}\text{Sr}_x\text{CuO}_4$ (LSCO) family, a convincing case for (predominantly dynamic or disordered) stripes can be made, based on elastic and inelastic neutron scattering^{1–5}, NMR and NQR^{6,7}. In other systems, the evidence is more ambiguous. In $\text{YBa}_2\text{Cu}_3\text{O}_{7-\delta}$ (YBCO), there is now^{8,9} clear evidence for incommensurate modulation of the inelastic magnetic neutron scattering near $\vec{Q} = (\pi, \pi)$, but so far only in underdoped $\text{YBa}_2\text{Cu}_3\text{O}_{6.6}$. Balatsky and Bourges¹⁰ find a broad commensurate peak, but the width of the peak scales with doping in exactly the same way as the incommensurability in LSCO, suggestive of an unresolved underlying incommensurability in YBCO, as well. Also, de Lozanne¹¹ finds direct STM evidence for incommensurate modulations (parallel to the chains) with a similar periodicity to the neutron data. Mook¹² has reported similar incommensurate neutron peaks in $\text{Bi}_2\text{Sr}_2\text{CaCu}_2\text{O}_{8+\delta}$ (BSCCO). Potentially stripe-related phonon anomalies have been reported in both LSCO¹³ and YBCO¹⁴. Doping with Zn seems to stabilize the stripe phase¹⁵. Photoemission evidence^{16,17} for stripes has been controversial^{18,19}.

Over the same doping regime, there is also evidence for a pseudogap, and it is an important problem to understand how both pseudogap and stripes can coexist.

In particular, photoemission finds a dispersion consistent with the two-dimensional (2d) energy bands, whereas in the stripe phase the magnetic stripes should be insulating, leading to a one-dimensional (1d) dispersion along the charged stripes.

The presence of stripe phases raises important issues of how energy dispersion and even Fermi surfaces can be well defined concepts in the presence of fluctuating stripes. An important insight into this problem is the finding by Salkola, et al. (SEK)²⁰ that a well-defined average dispersion persists even in the presence of strongly fluctuating stripe order. However, in that paper, and a related calculation²¹, the stripes were modelled by a charge density wave like order, with sinusoidally varying hole density. Several unrestricted Hartree-Fock^{22–25} or slave boson²⁶ calculations find evidence for much sharper density variations. The present paper analyzes a phase separation scenario, modelling the stripes as associated with free energy minima at two characteristic hole densities. This allows the doping dependence of the stripes and the resulting photoemission spectrum to be analyzed.

It is found that long-range stripe order can persist even in the presence of Coulomb interactions. The resulting dispersion is clearly recognizable as a superposition of the magnetic and charged stripe dispersions, with superimposed minigaps due to the stripe order. These dual dispersions provide a natural interpretation for the experimentally observed photoemission dispersions, tying together results on LSCO, BSCCO, and $\text{Sr}_2\text{CuO}_2\text{Cl}_2$ (SCOC). In the model, the 1/8 anomaly can be understood as a form of quantum critical point (QCP), associated with a crossover between a magnetic stripe dominated regime and a charged stripe dominated regime. Within the latter regime, the (π, π) spin gap in YBCO is related to the behavior of a two-leg ladder (isolated magnetic stripe).

Remarkably, within the charge stripe dispersion, a clear signature of the two-dimensional Van Hove singularity (VHS) persists, down to the limit of a single, two-Cu wide stripe. There is a strong coupling of the minigaps with this VHS, leading to a novel *stripe-induced VHS splitting*. The doping dependence of this splitting closely resembles that of the pseudogap.

The paper is organized as follows. Section II shows that a low hole doping of the charged stripes, $x_0 \sim 0.25$ is not only compatible with experiment, but also makes sense theoretically, in terms of kinetic-energy stabilized stripes. The models for the magnetic and the charged stripes are introduced in Section III, along with a discussion of long-range Coulomb interaction. Section IV gives the results of the stripe calculations, which self-

consistently determine the hole distribution. The doping dependence of the dispersion is presented, for varying strengths of Coulomb repulsion. Finally, the effect of an additional (ferromagnetic) interaction on splitting the VHS degeneracy on the charged stripes is discussed. In Section V, these results are compared to experiment, and a consistent model of the photoemission in LSCO and BSCCO is presented. Section VI points out that the model has a QCP – actually, a series of ‘magic doping’ QCP’s, of which the simplest is the 1/8 anomaly. To illustrate the resulting crossover, an additional calculation is presented in Section VII, showing how the doping dependence of the spin gap in YBCO can be understood. Possible explanations are also presented for the saturation of the incommensurability δ vs x found by Yamada, et al.²

Section VIII includes discussions of the interpretation of the peak-dip-hump structure in BSCCO, the new stripe-VHS spitting pseudogap, a discussion of Fermi surfaces and remnant Fermi surfaces in the stripe phase, and comparison with earlier calculations. A summary of the principal conclusions of this work is given in Section IX.

II. FRACTIONALLY-OCCUPIED STRIPES

A. Comparisons with other Oxides

Stripe arrays have now been found in a number of oxides, most notably nickelates and manganites. The similarities of cuprates with nickelates are particularly close: in both systems, the charged stripes act as antiphase boundaries for the magnetic stripes, and in both, the charge order arises at higher temperature than the magnetic order^{1,27}. The nickelate stripes run diagonally (with respect to the Ni-O-Ni bonds); this is also true of the LSCO stripes, in the spin glass regime²⁸, $x \sim 0.04-0.06$. However, in the superconducting regime, $x > 0.06$, the cuprate stripes are generally horizontal and vertical.

One striking difference is that in the nickelates and manganites, the charged stripes correspond to integer doping (one hole per Mn or Ni), leading to simple patterns^{29,30} of commensurate stripe arrays. There are prominent phase transitions at rational fractions, 1/2, and 1/3, corresponding to holes on every n th row, with evidence for commensurability locking in between (i.e., the 1/3 phase persists in an extended doping range about $x = 1/3$.) Consistent with integer filling, the phases are all insulating³¹. In contrast, in the cuprates the phases are all conducting or weakly localized, and the only fraction which appears prominently is 1/8.

In the present paper, a simple explanation is proposed for this distinction. The charged stripes are fractionally doped, with approximately 1/4 hole per Cu (hence explaining the finite conductivity). The magical 1/8 doping

would then correspond to the simplest ‘commensurate’ pattern of these stripes.

The stability of the stripe phase decreases in the sequence manganites, nickelates, cuprates. Thus, while there are beautiful electron microscopic images of long-range stripe order in the manganites³⁰, stripes in the cuprates are mainly fluctuating, with only short-range order. Within the present model, this pattern is readily understood, since the charged stripes are stabilized by CDW instabilities; this is similar to models for the nickelates and manganites³². The strength of this instability can be estimated by comparing the strength of electron phonon coupling, which follows the same sequence: manganites (with well-defined Jahn-Teller polarons), nickelates³³, cuprates. It is only in the cuprates where the interaction is so weak that a fractional occupation can be stabilized, and it is only in the cuprates that the stripe formation is so weak that superconductivity can successfully compete.

B. Origin of Fractional Occupation

Hartree-Fock calculations²² of the tJ model find that the holes condense onto domain walls between antiferromagnetically ordered domains, producing fully occupied stripes – one hole per Cu. However, neutron diffraction¹ finds a charge modulation of periodicity four Cu atoms at $x = 0.125$, which implies only 1/2 hole per cell. Tranquada, et al.¹ suggested a model for the charged stripes, based on their experience with stripes in nickelates. The hole-doped stripes are one cell wide, and have a hole on every other site. A microscopic model for such a domain wall can be derived³⁴ by incorporating a charge-density wave (CDW) instability along the stripes, treating them as one-dimensional metals. However, such states with integral hole doping are likely to be insulators, as is the case in the stripe phases of the nickelates³¹, whereas the cuprates are either conducting or weakly localized.

Moreover, fractional hole occupation would seem to be more natural for the tJ and Hubbard models, since the energy of doped holes is lowered by finite hopping t in a partially filled band. Visscher³⁵ and Nagaev³⁶ showed that the holes enhance their kinetic energy by creating local ferromagnetic domains (ferrons) in which they are free to hop. This leads to a preferred hole density, x_f inside the ferron domain. In a two-dimensional, tJ version of the model (letting $\hbar^2/2m \rightarrow ta^2$, with a the lattice constant),

$$x_f = \sqrt{\frac{zS^2J}{\pi t}} \simeq 0.334, \quad (1)$$

with $z = 4$ the number of nearest neighbors of a given Cu, and I have assumed $J/t = 0.35$. A similar result was found by Nayak and Wilczek³⁷. Nagaev’s model is a large- S theory, and Emery and Kivelson³⁸ extended it

to $S = 1/2$, although they did not address the issue of x_f . Auerbach and Larson³⁹ showed that a single doped $S = 1/2$ hole will spread out over a ferromagnetic domain covering 5 lattice sites, suggesting a comparable value for x_f , > 0.2 holes per site, on average (since the hole has a higher probability of being on the central atom). Recent density matrix renormalization group (DMRG) calculations of the tJ model undertaken by White and Scalapino (WS)^{40,41} find charged stripes which are two Cu's wide, with an average hole doping of 0.25 hole per Cu on the charged stripes. These calculations are further discussed in Appendix A.

Since the charged domains are stabilized by the hole kinetic energy, it is plausible that enhancing the kinetic energy could enhance the stability of the hole-doped stripes. Thus, in a generalized Hubbard model, with next-nearest neighbor hopping t' , it is found that a macroscopic ferromagnetic phase is stabilized in the vicinity of the Van Hove Singularity (VHS)⁴². Moreover, an extended Hartree-Fock analysis²⁵ finds phase separated states smoothly evolving between the AFM and FM regions, from a single magnetic polaron to FM stripes to a uniform FM phase.

However, such ferromagnetic domains have not been observed in the cuprates. Nevertheless, there are alternative VHS routes to fractionally-occupied stripes. The large density of states (dos) associated with a VHS can drive a large number of competing electronic instabilities^{43,44}, and it was early suggested that this could be the origin of nanoscale phase separation in the cuprates⁴⁵. In particular, it was demonstrated that strong electron-phonon coupling could stabilize a charge-density wave phase near the VHS^{45,46}.

C. Viability of VHS Models

In any model of stripe phase formation based on Fermi surface features, there is a fundamental question of self-consistency: do the features persist in the limit of an isolated stripe? Can one still recognize bulk features of the band structure and Fermi surfaces of the phases forming the stripe array? This is one of the main issues that this paper resolves: even in the limit of nanoscopic stripes, the band structure is recognizably a superposition of the structures of the two end phases. The main role of stripe order is to introduce miniband gaps into this structure.

In the particular case of the VHS's, there were a number of preliminary indications which suggested such an affirmative answer. First, SEK²⁰ found that an average dispersion persists in the presence of fluctuating stripes; the resulting 'flat bands' are a signature of the VHS. Secondly, within a group theoretical (SO(6)) model⁴⁴, the Van Hove instabilities all remain well-defined on a single plaquette of 2×2 Cu atoms, so *a fortiori* they should remain well defined on a 2-leg ladder. Indeed, Lin, Balents, and Fisher⁴⁷ found an SO(8) group controlling the

physics of the 2-leg ladder. When one eliminates⁴⁸ certain one-dimensional operators (which break the $k \rightarrow -k$ symmetry along the ladder), one is left with the same SO(6) group introduced earlier for the VHS. Such a correspondence would fail for a single-leg ladder.

Hence, the present model is restricted to stripes which are an even number of cells (or Cu atoms) wide. This point was previously postulated for the magnetic stripes, in terms of spin gaps associated with even-legged ladders⁴⁹. Moreover, WS find two-Cu wide charged stripes in their DMRG calculations⁴⁰. With this assumption, it is found that a VHS-like feature can be clearly resolved near the Fermi level in the stripe phases. Moreover, the stripes provide a new mechanism for VHS splitting – minigaps – which can generate a pseudogap with the correct doping dependence.

III. MODELING THE STRIPES

While the stripes are likely to be strongly fluctuating, the band structure modifications should be strongest, and can be analyzed in most detail, in an ordered stripe phase. Hence, the present calculation assumes perfectly ordered stripe phases to describe this 'worst case' scenario. It will be assumed that there are two preferred hole densities, $x \sim 0$ on the magnetic stripes, and $x_0 \sim 0.25$ holes per Cu on the hole-doped stripes. Coulomb effects lead to additional charge relaxation, and a more uniform distribution of charge, Section III.D.

A. Model for the Magnetic Stripes

In the insulating phase, a variant of the spin-density wave (SDW) model studied by Schrieffer and coworkers^{50,51} is used. This model works surprisingly well in the large-U limit⁵², reproduces the spin wave spectrum of the Heisenberg model, and has served as the basis for a number of extended treatments of correlation effects^{53–56}. For realistic parameters (t, t', U), the model has a Mott-Hubbard gap of 2eV, and can reproduce the dispersion found in the oxycloides^{57,58}, Appendix B.

The dispersion of the one-band model can be written

$$\epsilon_k = -2t(c_x + c_y) - 4t'c_xc_y, \quad (2)$$

with $c_i = \cos k_i a$. Writing $\epsilon_{\pm} = (\epsilon_k \pm \epsilon_{k+Q})/2$, the eigenvalues in the presence of a Hubbard U become

$$E^{\pm} = \epsilon_{\pm} \pm \sqrt{\epsilon_{\pm}^2 + \bar{U}^2}, \quad (3)$$

where $\bar{U} = Um_Q$. In the limit $\bar{U} \gg t$, the lower Hubbard band may be approximated

$$E^- = -\bar{U} - 4t'c_xc_y - J(c_x + c_y)^2, \quad (4)$$

with $J = 2t^2/\bar{U}$. The parameters can be determined by fitting to the observed photoemission dispersion in SCOC. For simplicity, one can use analytical expressions for the parameters at three k -space points: $E^-(\pi/2, \pi/2) = -\bar{U}$, $E^-(\pi, 0) = -\bar{U} + 4t'$, $E^-(0, 0) = -4t' - \sqrt{U^2 + 16t'^2}$ (Eq. 4 is not sufficiently accurate for this purpose). The fit yields $t = 325\text{meV}$, $\bar{U}/t = 2.5$, and $\tau = 2t'/t = -0.552$. Solving the gap equation at half filling, this value of \bar{U} corresponds to $U/t = 6.03$, $M_Q(x = 0) = 0.414$ (Fig. 1), or 83% of the classical value.

For these parameters, $M(x)$ is multivalued for $x \geq 0.38$. This implies that the magnetic to non-magnetic transition is first order. This is discussed further in Appendix B. However, this density is rather higher than expected for charged stripes. In LSCO, the VHS splitting seems to terminate near $x = 0.26^{59,60}$, and similar results are found below for YBCO. In a number of models^{46,42}, the AFM instability is replaced by a second instability, driven by splitting the VHS degeneracy. Note that the bare ($U = 0$) VHS falls at $x = 0.25$ for $\tau = -0.559$, very close to the value needed to explain the dispersion in the insulating phase.

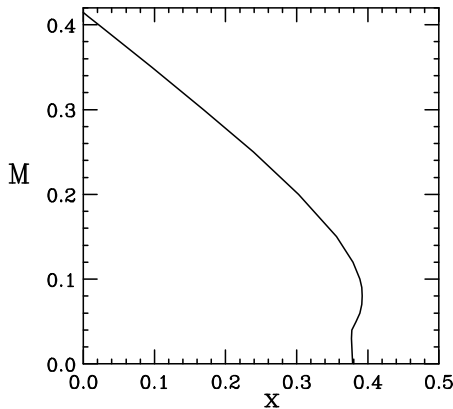


FIG. 1. Doping dependence of magnetization in the SDW model.

If M_Q is interpreted as the long-range antiferromagnetic order parameter, then the model does a poor job in describing the temperature and doping dependence of the Néel transition⁶¹, T_N , yielding $T_N \sim U/4$. Figure 1 shows that, while M_Q is strongly renormalized by doping, the mean-field theory underestimates the rapidity of the falloff of T_N with x . However, the mean-field results are best reinterpreted as representing *short-range order* – the magnetic fluctuations – and hence the renormalization of the *splitting* into upper and lower Hubbard bands. In this case, the mean-field calculations are in good agreement with exact diagonalization calculations⁶². The fact that the gap is much smaller in the doped phase is consistent with the experimental observation⁶³ that the upper Hubbard band rapidly disappears with doping.

B. Model for the Charged Stripes

It is assumed that the hole-doped stripes are stabilized by splitting the VHS degeneracy, at the doping $x_0 \sim 0.25$ where the VHS falls at the Fermi level. An earlier slave boson calculation⁴⁶ demonstrated that electron-phonon coupling could provide that stabilization energy, even in the presence of strong correlation effects. A ferromagnetic interaction⁴² can produce similar splitting.

While the earlier electron-phonon calculation involved a three-band model, here a simpler one-band model will be adopted. A parametrized form of the free energy vs doping found in the self-consistent calculation⁴⁶, Fig. 2, will be assumed, to stabilize the stripe phase. It is convenient at present to *not* introduce any mechanism to split the VHS degeneracy. This allows a definitive answer to an important question: can evidence for the VHS still be found in the presence of a well-defined stripe phase? The answer is a clear yes: the resulting dispersion is a superposition of the magnetic dispersion and the charged stripe dispersion, with recognizable VHS feature. What is more, the stripe phase minigaps provide a *new mechanism of VHS splitting*, with a doping dependence comparable to the experimental pseudogap.

A very simple doping dependence of the parameters is assumed. From Eqs. 2-4, for finite U t is renormalized by a factor t/Um_Q , Fig. 1, so the increase of t with doping is accomplished by the decrease in m_Q , the ordered moment. We will thus make a simple *Ansatz* that the only effect of doping is to renormalize

$$m_Q \rightarrow m_Q(1 - x/x_0). \quad (5)$$

Since the stripes are predominantly near the limiting states $x = 0, x_0$, the detailed nature of the intermediate states is relatively unimportant. As noted above, Eq. 5 neglects the gap on the charged stripe; in Section IV.D, a ferromagnetic interaction will be included on the charged stripes, to show that the VHS splitting is preserved in the striped phase.

C. Free Energy Minima

To stabilize the stripe densities at the values $x = 0$ for magnetic stripes, and $x = x_0 = 0.25$ for the charged stripes, the following free energy is introduced, based on the results of slave boson calculations for the three-band model⁴⁶:

$$f_0(x) = \mu_0 x \left(1 - \frac{x}{x_0}\right)^2, \quad (6)$$

for $x > 0$. (At $x = 0$ there is a cusp-like minimum, associated with the Mott gap in the chemical potential.) Figure 2 illustrates the free energies calculated in a three-band slave boson calculation for competing magnetic (here a flux phase – dashed line) and charged (CDW – solid line) phases, and a fit of these to Eq. 6,

with $\mu_0 = 0.9eV$. For these calculations, $x_0 = 0.16$ was assumed. This should be compared to Fig. 2 of Ref. 46. Note that there is an error in the caption of that figure: the CDW phase there corresponds to a weaker coupling, $V_{ep} = 0.6eV$.

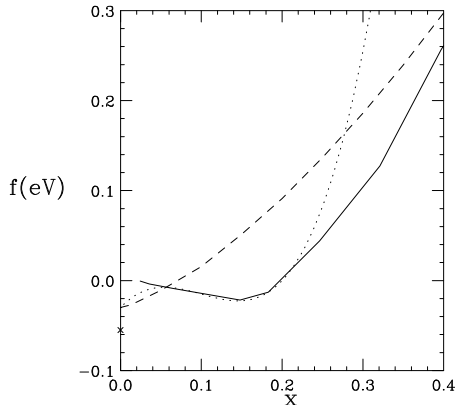


FIG. 2. Free energy calculated in a three-band slave boson theory⁴⁶, showing phase separation between a flux phase (dashed line) and a CDW phase, with $V_{ep} = 1eV$ (solid line). Dotted line is a fit to Eq. 6.

Equation 6 is a convenient form for parametrizing the confining potential of a striped phase. It has only two parameters, x_0 and μ_0 , or equivalently, $f_m = 4\mu_0 x_0/27$, the maximum free energy barrier, at $x_0/3$. In the present stripe phase calculations, these parameters are taken as $x_0 = 0.25$ and $\mu_0 = 0.312eV$, or $f_m = 11meV$. This value corresponds to $V_{ep} = 0.6eV$ of Ref. 46, and allows us to see that even a relatively modest confining potential can stabilize the stripe phase against the Coulomb potential. This free energy corresponds to an additional chemical potential

$$\mu(x) = -\mu_0 \left(1 - \frac{x}{x_0}\right) \left(1 - \frac{3x}{x_0}\right) \quad (7)$$

for $x > 0$. In the calculations, this $\mu(x)$ is added to the potential on each row, and the local density adjusted until self-consistency is attained.

At $x = 0$, μ has a discontinuity, the Mott-Hubbard gap. Hence, at this point, the Fermi level can take on any value inside the gap. To model this in a computationally stable manner, the discontinuous step in μ is replaced by a linear ramp, connecting the values of μ at $x = -0.01$ and $x = +0.01$, and assuming $\mu(x = -0.01) = -\mu(x = +0.01)$. Thus, when the calculation finds $|x| < 0.01$, it generally implies that the Fermi level is in the gap of the magnetic stripes. However, due to hybridization with holes in the charged stripes, it is possible to have a well-defined Mott gap, with a small doping $x > 0$ on the magnetic stripes (typically, $x \leq 0.05$).

D. Madelung Energies of Stripes

We will assume for simplicity that all stripes, both magnetic and charged, are an even number of cells wide. This means that only a relatively small number of stripe configurations are involved in the doping range of interest. For instance, labelling the stripe configuration by m, n , where m is the width of a magnetic stripe and n the width of a charged stripe, we will explore in detail the pure phases $m, n = 6, 2$ ($x = x_0/4 \simeq 0.0625$, if $x_0 \simeq 0.25$), $4, 2$ ($x = x_0/3 \simeq 0.0833$), $2, 2$ ($x = x_0/2 \simeq 0.125$ – the $1/8$ phase), $2, 4$ ($x = 2x_0/3 \simeq 0.167$), and $2, 6$ ($x = 3x_0/4 \simeq 0.1875$). Intermediate dopings would correspond to mixed phases. For each of these phases, we assume that there can be different dopings on each row; by symmetry, there can be $(m+n)/2$ inequivalent rows for the m, n -phase.

In the presence of charging, it is the electrochemical potential μ_e and not the chemical potential, μ , which is constant. For electrons, $\mu_e = \mu - eV$, where V is the electrical potential. Given the average hole density on each row, V can be calculated as a Madelung sum. For each configuration, the Madelung sum can be calculated for each row. Actually, since the overall chemical potential must be adjusted to fix the total hole density, all that need be calculated is the difference in Madelung potential between the different rows. This is calculated by assuming a pure Coulomb interaction, screened by a static dielectric constant, ϵ . The on-site term is neglected, having already been included as U .

The various Madelung constants can be expressed as follows. For the $(6,2)$ stripe, label the rows 1,2,3,4, with 4 = the charged stripe, and 1 (3) = the magnetic rows farthest from (nearest to) row 4. Let V_i be the Madelung potential for the i th row, $\tilde{V}_i = (V_i - V_1)x_0$, x_i the hole doping of the i th row, and $\tilde{x}_i = (x_i - x_1)/x_0$. Then

$$\tilde{V}_i = V_0 \sum_j K_{ij} \tilde{x}_j, \quad (8)$$

where the K^m matrices have been calculated numerically, with results listed in Table I, for the cases $(m,2)$, $m = 2,4,6$. The constant $V_0 = 2x_0 e^2/(\epsilon a) = 0.914eV/\epsilon$, for $x_0 = 0.25$.

Table I: Madelung Matrices

K_{ij}^m	$j = 2$	3	4
$K_{2j}^6 =$	-0.4110	0.5365	0.347
$K_{3j}^6 =$	-0.3466	0.4721	1.230
$K_{4j}^6 =$	-0.8831	0.8831	1.702
$K_{2j}^4 =$	-0.3082	0.6951	
$K_{3j}^4 =$	0.	1.082	
$K_{2j}^2 =$	0.1256		

The stripe phase is stable only if the dielectric constant is large enough: recent calculations⁶⁴ suggest $\epsilon > 5$ is sufficient. The large static dielectric constant of the cuprates, $\sim 40 - 80$ ⁶⁵, is a sign of strong electron-phonon

coupling. This large coupling makes it difficult to accurately estimate the strength of the Coulomb interaction. The d.c. dielectric constant will be anisotropic and, most probably, dispersive, on the length scale of the stripes. Since interlayer contributions to screening can be important (e.g., apical oxygens, bilayer coupling), this is one parameter which could easily have a strong material dependence.

While the above procedure should approximately capture the long range part of the Coulomb interaction, it will likely overestimate the hole-hole repulsion for nearest neighbors. This can be thought of in terms of a correlation hole having two components. First, we are assuming that a hole on a given site interacts with a fractional hole (the average doping) on all other sites. Clearly, part of the hole population on the nearest neighbor sites is actually generated by the hopping of the given hole, hence should not be counted in the Madelung sum. Moreover, there is likely to be a real correlation hole, as neighboring charges readjust to avoid the given hole. However, these terms are associated with CDW formation, which will not be dealt with explicitly here.

IV. RESULTS

A. Absence of Coulomb Interaction

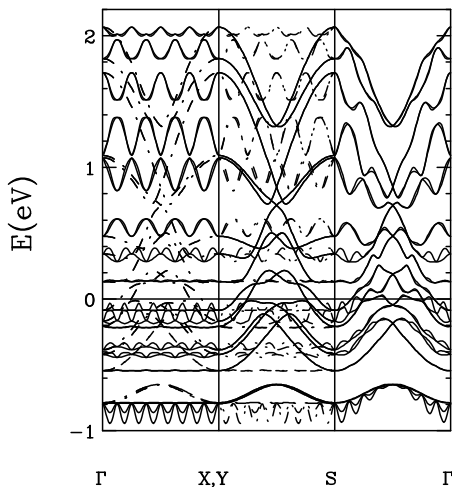


FIG. 3. Dispersion of 2,6 structure. Solid lines $\Gamma \rightarrow X \rightarrow S \rightarrow \Gamma$; dot-dashed lines $\Gamma \rightarrow Y \rightarrow S$. Here, Y is along the stripes, X is across them.

Figure 3 illustrates the band dispersion for a 2,6 structure ($x = 0.1875$), in the absence of long-range Coulomb effects. The hole doping on each layer is self-consistently adjusted to allow for inter-row hopping processes, and the Fermi level is adjusted to account for the overall doping. In the absence of long-range Coulomb effects, the doping is close to the nominal values. Numerical results will

be discussed in the following subsection, which will show how they are modified by Coulomb interaction.

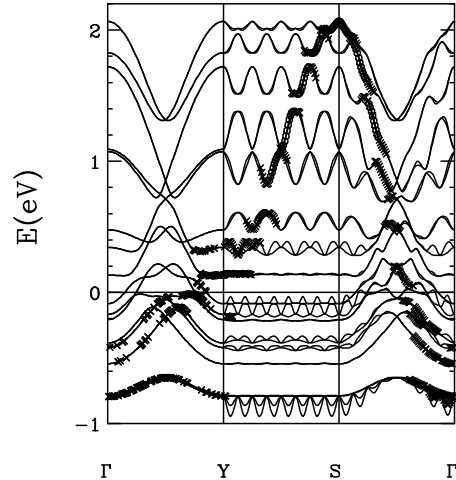


FIG. 4. Dispersion of 2,6 structure, but with structure factors.

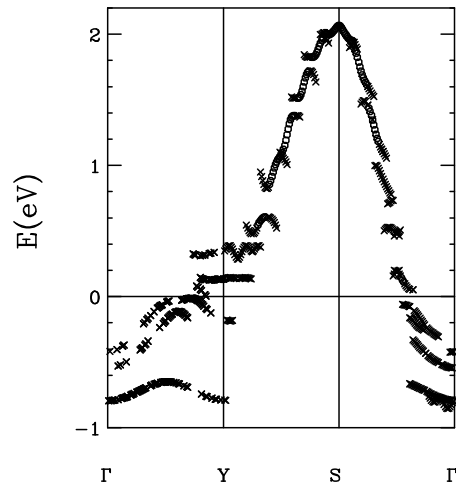


FIG. 5. Dispersion of 2,6 structure, parallel to the stripes.

The large number of bands is rather deceptive. It is equal to the number of Cu atoms in the large unit cell, doubled since the up and down spin bands are not degenerate. There would be the same number of bands *even if there were no stripes*. But in this case, only one band would satisfy Bloch's theorem. This band can be determined by looking at the structure factor – the overlap of the corresponding wave functions with $e^{i\vec{k}\cdot\vec{r}}$. Similarly, when stripes are present, the same structure factor determines which bands will be seen by photoemission. This is illustrated in Fig. 4, where the circles indicate a weight greater than 0.5, and the \times 's a weight between 0.5 and 0.1. For greater clarity, only the dispersions along $\Gamma \rightarrow Y \rightarrow S$ are shown. The dispersions along Y (parallel to the stripes) and X (transverse to the stripes)

are shown in Figs. 5 and 6, respectively. The resulting weights reveal a simple result: the envelope of the bands is approximately a superposition of the two limiting bands, at half filling and at optimal doping, with considerable fine structure associated with minigaps.

In the presence of stripes, the dispersion should be quasi one-dimensional. This is clearly seen in Fig. 3, where the dispersion along $\Gamma \rightarrow Y$ ($\Gamma \rightarrow X$) closely resembles that along $X \rightarrow S$ ($Y \rightarrow S$). However, with the structure factors included, the dispersions are quite distinct. Nevertheless, the minigaps are most prominent in the dispersions perpendicular to the stripes, $\Gamma \rightarrow X$, (Fig. 5), and $Y \rightarrow S$, (Fig. 6).

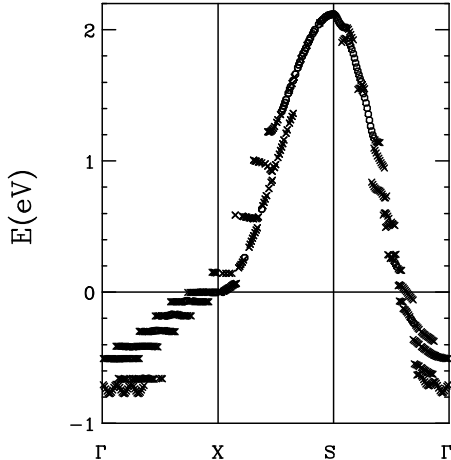


FIG. 6. Dispersion of 2,6 structure, transverse to the stripes.

Fig. 7 shows the doping dependence of the dispersion, illustrating the ‘projected’ dispersion of the charged and magnetic stripes. The projected charge stripe is found by plotting those points where the wave function spends $\geq 80\%$ of its time on the charged layers. The curves show the dispersions for a series of dopings, from $\Gamma \rightarrow X \rightarrow S \equiv (\pi, \pi)$. While the fine structure (minigaps) is strongly doping dependent, *the overall dispersion is not*, and is essentially identical to the dispersion of the uniform end phases. This is exactly what would be expected for *macroscopic* phase separation, even though at crossover the charge stripe is only two cells wide.

The figure shows that the dispersion is largely a superposition of two Fermi surfaces: one for the insulating magnetic stripes, one for the charged stripes: the small +’s (large circles) indicate $\geq 80\%$ of the wave function is on the magnetic (charged) stripe; the small diamonds indicate a mixture of both. Note that there is strong overlap in the region of the upper Hubbard band, while the magnetic lower Hubbard band (LHB) remains well defined at all dopings, and the charged stripes fill in the gap as doping increases.

It should be noted that once the charged stripes are reduced to two cells wide, at $x=0.125$, the dispersion re-

mains nearly unchanged as the doping is further reduced (e.g., at $x=0.0625$). Hence, an important aspect to understanding the strongly underdoped stripe phases will be to develop a good model for these limiting, two-cell stripes. As discussed below, there is an analogous magnetic stripe beyond the percolation crossover, which can be modeled as a two-leg ladder.

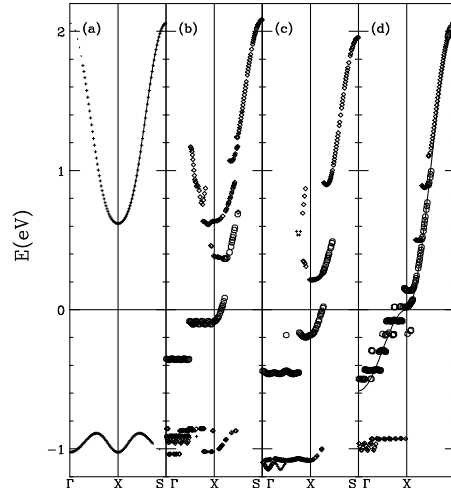


FIG. 7. Total dispersion from $\Gamma \rightarrow S$ for dopings: $x = 0$ (a), 0.0625 (b), 0.125 (c), 0.1875 (d), and 0.25 (solid line in d). Data in (a) were shifted upward by 0.16eV.

B. Coulomb Interaction

Inclusion of Coulomb interaction leads to fairly modest changes in the dispersion. Figure 7, with no Coulomb effects, should be compared to Fig. 8, with moderate screening $\epsilon = 15$. Careful inspection reveals that the charged bands are shifted to lower energy with respect to the magnetic layers, so that the lower Hubbard band is more fully hybridized with the charged layers. With reduced screening ($\epsilon = 5$) the bottom of the charged band actually falls below the magnetic lower Hubbard band. The layers near the Fermi level remain predominantly associated with the charged layers, so we may still loosely speak of charged bands and magnetic bands. Note that in every case, the Fermi level lies within the minigap closest to the Van Hove singularity. This provides a *new mechanism* for the opening of the pseudogap, as will be discussed further below.

Even in the absence of Coulomb interaction, the carrier density in a given row deviates somewhat from the free energy minima – here taken as $x=0, 0.25$ – due to the finite hopping probability. For the 2,6 structure, Figs. 3-5, the magnetic layers have $x=0.025$, and for the charged layers, moving away from the magnetic layer, the hole doping is 0.25, 0.24, and 0.24. Adding the Madelung potential raises the energy of the hole-doped stripes, and requires a shift of the Fermi energy

to compensate. However, since the magnetic stripes are gapped, this shift makes little difference to the hole population on these stripes, the corresponding layer populations being 0.026, 0.255, 0.25, and 0.22, for $\epsilon = 15$, Fig. 8. For larger Coulomb interaction, the deviation becomes greater, Fig. 9. The data display an interesting evolution: superimposed on a trend toward greater homogeneity, there is also a tendency to evolve into a (2,2) state. This can be understood from Table I: the Coulomb effects are smallest for this state, since the phase separation is restricted to the finest scale.

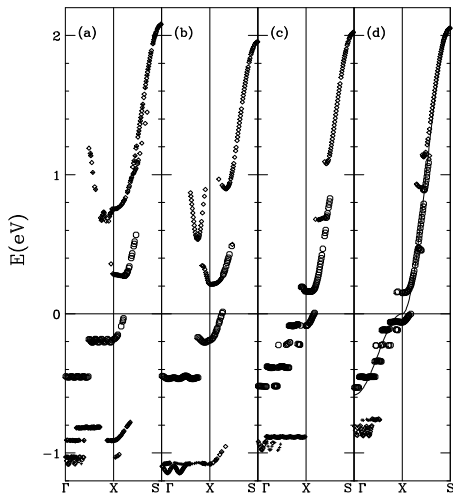


FIG. 8. Total dispersion corrected for charging ($\epsilon = 15$) from $\Gamma \rightarrow S$ for dopings: $x = 0.0625$ (a), 0.125 (b), 0.167 (c), 0.1875 (d), and 0.25 (solid line in d).

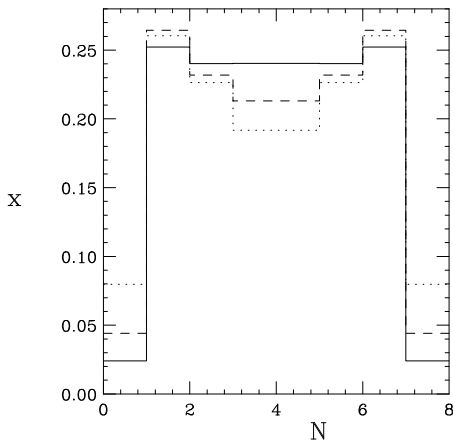


FIG. 9. Hole distribution on rows (labelled by N) of the 2,6 structure, for $\epsilon = \infty$ (i.e., no Coulomb interaction – solid line), 15 (dashed line), or 5 (dotted line).

This result is of potential relevance for LSCO: it is found experimentally that the incommensurability saturates near $1/8$ doping – here the crossover where the (2,2) phase is stable. The saturation could simply mean that

for LSCO, the Coulomb effects are large enough that the system locks into the (2,2) phase for all higher dopings.

There is a striking asymmetry about $1/8$ doping: in the (6,2) phase, Coulomb interaction makes very little difference. This is because of the sharp cusp instability at half filling, which keeps the hole doping fixed near zero in the magnetic stripes, whereas the shallower potential minimum near optimal doping allows more substantial density fluctuations.

These results will be discussed further in a later section. Two points are worth mentioning: first, the incommensurability saturation has so far only been observed in LSCO; and secondly, LSCO closely resembles the other cuprates in the doping range up to $1/8$, but for higher doping, T_c saturates at a much lower value.

C. Minigaps

Figure 8 shows the evolution of the minigaps with doping. A simple model provides a semiquantitative explanation of these results. The dispersion along $(0, 0) \rightarrow (\pi, 0)$ is discretized into n levels for n -Cu wide charge stripes. This bandwidth is $4(t+2t') \simeq 584 \text{ meV}$. If the minibands are equally spaced, the average gap should be $584/(n-1)$ meV. Actually, the net bandwidth changes some with doping, so a better formula is

$$\Delta_{av} = \frac{584 \text{ meV}}{n} \quad (9)$$

= 292 ($n=2$), 146 (4), or 97 (6) meV, to be compared with average values (Fig. 8) of 260 , 147 , and 94 meV, respectively. For the dispersion along $(0, \pi) \rightarrow (\pi, \pi)$, the same bands are present, but shifted by the dispersion along Y , and with total bandwidth $4(t-2t')$.

For fluctuations in the stripe spacing, there will be a tendency to average over the various dispersions in Fig. 8. This will tend to wash out most of the minigaps, since they are shifted in energy as the stripe width changes. However, since there is always one gap present near the Fermi level, this gap should survive averaging. For the uniform stripe phases of Fig. 8, this 'pseudogap', or distance between the Fermi level and the nearest $(\pi, 0)$ minigap, follows the same scaling as Eq. 9, $\Delta_p = 364/n$ meV.

D. Ferromagnetic Stripes

Figure 7 shows that, beyond the percolation crossover a clear remnant of the bulk VHS is visible in the striped phase dispersion. In Figure 10, it can be seen that splitting this VHS degeneracy produces a clear pseudogap-like splitting of the dispersion near $(\pi, 0)$. It is this lowering of a large density of states that has been postulated to stabilize the charged stripes, and the figure clearly shows that the mechanism remains active even in the striped phase.

For the calculations in the figure, it was assumed that the antiferromagnetic phase is stable only up to a doping $x_0/3$, while for larger doping a ferromagnetic instability wins out. The ferromagnetic dispersion is also given by Eqs. 2-4, but with $q = (0, 0)$ instead of $Q = (\pi, \pi)$. For the same value of U , the equilibrium M has the form shown in Fig. 11, which was approximated by $M = 0.4 - 0.5|x - 0.2|$.

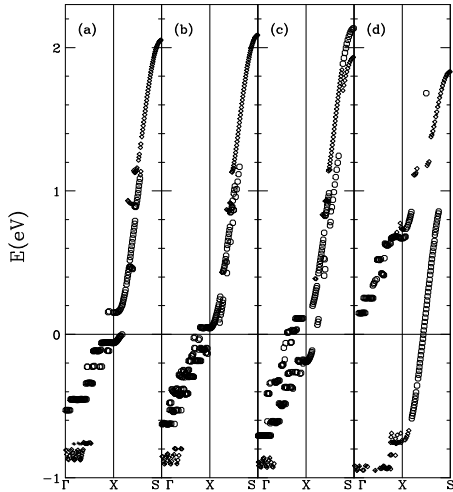


FIG. 10. Dispersion along X for a ferromagnetic instability on the charged stripes, for $x = 0.1875$ (2,6), and different degrees of magnetization M , as discussed in the text.

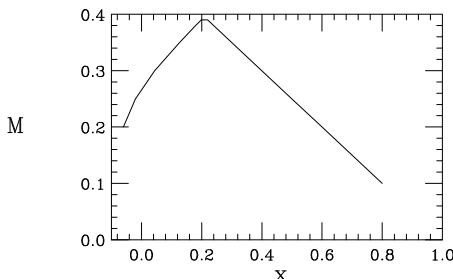


FIG. 11. Doping dependence of the magnetization M for a ferromagnetic instability.

It should be noted that the doping dependence depends sensitively on the choice of parameters; these values are taken for illustrative purposes only. Figure 10d shows the dispersion of the self-consistent solution with the full $M(x)$, while the other frames show a reduced M of $1/5$ (c), $1/10$ (b), or 0 (a). Since the parameters were chosen to have the VHS in frame (a) centered on the Fermi level, the pseudogap opens approximately symmetrically about the Fermi level.

This should not be taken as evidence that the charged stripes really are ferromagnetic, only as an example of yet another kind of instability that is driven by the VHS. The figure illustrates that one can distinguish different insta-

stabilities, but one must carefully analyze secondary characteristics, since the opening of the pseudogap near $(\pi, 0)$ is common to a variety of instabilities. In the present instance, a ferromagnetic instability does not double the unit cell, so the ghost dispersion beyond $(\pi, 0)$ is absent, in contrast to experiment (see Fig. 24 below). Moreover, the splitting of the spin up and spin down bands should lead to extra structure most clearly seen (below the Fermi level) near Γ , which is not found experimentally.

V. COMPARISON TO EXPERIMENT

A. Photoemission in LSCO

The doping dependence of the photoemission spectra in LSCO⁶⁶ is strikingly different from that in BSCCO⁶⁷. In this section, it will be shown that *both* spectra can be interpreted in terms of stripe phases, with stronger fluctuation effects in BSCCO.

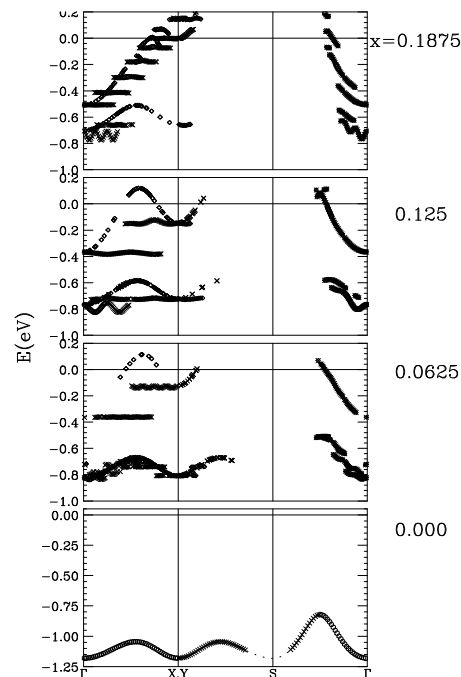


FIG. 12. Superposition of X and Y dispersions for, from bottom to top, $x = 0, 0.0625$ (6,2 structure), 0.125 (2,2), and 0.1875 (2,6).

Since no-one has yet succeeded in making a single-domain sample, the photoemission should best be compared with a superposition of the X and Y dispersions. Figure 12 illustrates how the pattern changes with doping. The following features should be noted: (1) there is always a prominent flat band near $(\pi, 0)$, which tends to shift further below the Fermi level with increased underdoping. (2) By construction, the dispersion at half filling matches that found in SCOC. (3) The evolution with

doping is not smooth, but crosses over from the SCOC band near half filling to a more metallic band near the Fermi level at higher dopings. The overall doping is quite similar to the experimental results of Ino, et al.⁶⁶ (see particularly their Fig. 3), confirming the suggestion that stripes are better developed in LSCO than in BSCCO.

Figure 13 compares the $(\pi, 0)$ photoemission peak positions for LSCO⁶⁶ with the present calculations. Results for BSCCO⁶⁸ are also shown; these will be discussed in the following subsection. In LSCO, there are two main features: one (\times 's) is near -0.6eV, with a dispersion similar to that in the magnetic insulator SCOC, and with a nearly doping-independent binding energy. The second feature (open circles) is a gap close to E_F with larger doping dependence. Qualitatively, these features are similar to the hump and peak features in BSCCO, but with larger binding energies. These two features can be correlated with two prominent gap-like features in the calculations: the magnetic gap associated with the lower Hubbard band on the magnetic stripes, and the charge stripe gap, associated with the miniband closest to the Fermi level. The calculated gaps are larger, since the energy scale has been chosen to agree with the magnetic gap in SCOC, yielding a value -1.2eV at half filling, but the overall doping dependences are quite similar to LSCO. This similarity is brought out most clearly by plotting the calculated gap values divided by two (diamonds and suns).

B. Photoemission in BSCCO

1. Below T_c

The photoemission in BSCCO is strikingly different from the above results, yet also provides evidence for stripes, but of a more fluctuating form. In BSCCO, there is a remarkable evolution of the photoemission with temperature, particularly on passing through T_c . Above T_c , the spectra are very broad, with a single broad peak near $\pi, 0$ representing the normal-state pseudogap. Below T_c , the spectra sharpen and split into two features, commonly referred to as a 'peak' near E_F , with a 'hump' at lower energies, close to the normal state pseudogap; between the peak and hump, there is a clear 'dip' in intensity, below the level in the normal state. Recently, systematic studies of these features in both tunneling⁶⁹ and photoemission⁶⁸ were presented. Most strikingly, photoemission finds these two peaks in the same direction of k -space, a feature which is very suggestive of phase separation.

Here, it will be assumed that the photoemission is dominated by stripe effects, and the main role of superconductivity is to suppress fluctuations. (The clear sharpening of the spectra below T_c , even in a range away from any gaps, is demonstrated in Ref. 70.) The analysis will be in two parts. First, the low-T spectra will be

compared with those of LSCO. Then the role of fluctuations in producing the high-T smeared spectra will be discussed.

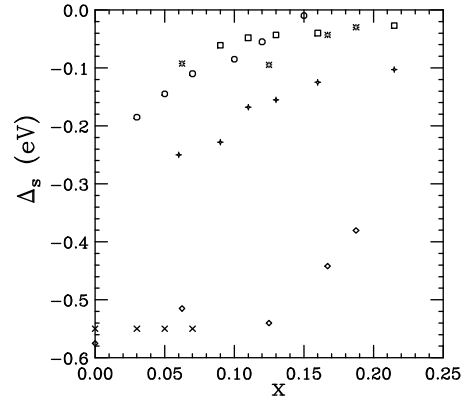


FIG. 13. Pseudogaps at $(\pi, 0)$ in LSCO⁶⁶ (\times 's, open circles) and BSCCO⁶⁸ ($+$'s = hump, squares = peak) compared to calculated Mott gap (diamonds) and minigap (suns); the calculated values are reduced by a factor of two. At the highest doping, the Mott gap does not show much intensity near $(\pi, 0)$; what is plotted is energy of the corresponding dispersion nearest to $(\pi, 0)$.

In Figure 13 the low-temperature photoemission peaks⁶⁸ of BSCCO are compared to those of LSCO. The 'peaks' (squares) are in reasonable agreement with the near- E_F pseudogap in LSCO (circles), and with the calculated minigaps. On the other hand, the 'humps' ($+$'s) are considerably closer to the Fermi level than the magnetic stripe feature in LSCO (\times 's); compared to theory, the overall offset is different, but the doping dependence is similar. Nevertheless, identification of the hump with the antiferromagnetic Mott gap feature is compelling. Laughlin⁶⁷ clearly showed that the photoemission data evolve with doping to match the SCOC spectrum at half filling. A detailed fit shows that this only works if the dispersion at $(\pi/2, \pi/2)$ touches the Fermi level – unlike SCOC, where there is a ~ 0.8 eV gap or LSCO with a ~ 0.3 eV gap. In Appendix B it is shown that the complete doping dependence of the hump is well described by simply doping into the lower Hubbard band of the antiferromagnet.

There is a clear progression in the magnetic stripe separation from the Fermi level, from SCOC (and the present magnetic stripe calculation) to LSCO to BSCCO. It is likely that this is due to stripe fluctuation effects, since as the band moves closer to E_F , there will be progressively more holes on the magnetic stripes. Further evidence for this interpretation lies in the high-T BSCCO spectra, where the peak and hump collapse into a single feature, which continues to resemble the magnetic dispersion (Appendix B) and is even closer to E_F than the hump. The conclusion that fluctuations are strongest in BSCCO is consistent with the fact that incommensurate magnetic modulations have not yet been clearly seen in

BSCCO.

2. Above T_c

In BSCCO, there is a sudden change of the photoemission spectrum at T_c : a single broad feature above T_c splits into a peak-dip-hump structure below T_c . This is here assumed to be mainly a fluctuation effect: above T_c , both features are assumed to be present, but the line broadening is so large that they strongly overlap. Below T_c , fluctuations are greatly suppressed, and the linewidth broadening Γ is reduced by over an order of magnitude⁷¹, so a truer picture of the spectra is obtained. Superconductivity will also renormalize the gap on the charged stripes (as discussed for a related model in Ref. 72), but this will be a secondary effect.

In LSCO, the photoemission spectra were observed⁶⁶ only in the superconducting state, due to surface degradation at higher temperatures. However, the stripes are clearly better defined in LSCO (the two gap features are more clearly separated) even though T_c is considerably lower, so it is quite possible that the split spectral peaks persist above T_c .

Ref. 72 (Fig. 19) showed that the changes in BSCCO at T_c can be interpreted in terms of enhanced fluctuations in the normal state; a similar calculation was presented by Chubukov and Morr⁷³. To explain the observed BSCCO photoemission, it is assumed that the local hole density is inhomogeneous, and the photoemission can be described as a superposition of the spectra of different densities. The spectral broadening in the superconducting state is taken to have the normal-state value for energies greater than twice the superconducting gap, Δ_s , but to have a ($5\times$) smaller value at lower energies. This spectral sharpening can produce a double-peaked photoemission spectrum, even if the density distribution is single peaked. A detailed comparison with experiment, Fig. 4a of Ref. 68, will require a more detailed model of the fluctuations.

There is an alternative class of models for the peak-dip-hump structure. In this picture, the dispersion is split because the holes strongly interact with some bosonic excitation. Abanov and Chubukov⁷⁴ have related the dip position to the resonance peak seen in neutron scattering. It is tempting to speculate that both views are approximately correct, and that the bosonic excitations originate from stripe fluctuations.

VI. DUALITY CROSSOVER: A PERCOLATION QCP

There is considerable evidence for a quantum critical point (QCP) in the cuprates⁷⁵. However, the QCP is at too high a doping to be a conventional Néel QCP, which should fall at a doping near $x \simeq 0.02$, where $T_N \rightarrow 0$.

Moreover, in undoped La_2CuO_4 and other spin-1/2 antiferromagnets, no evidence is found for a high-T crossover to a quantum critical state⁷⁶. The QCP also lies significantly below optimal doping⁷⁷. The QCP has also been associated with the termination of stripe ordering⁷⁸, but again, the doping seems wrong: stripes persist well above optimal doping in Nd-substituted LSCO, as does the pseudogap. The evidence seems to point to the 1/8 anomaly playing a role: Hunt, et al.⁶ find a significant crossover, which they suggest is the end of the stripe regime, at $x \simeq 0.125$, and they further suggest that the high-field metal-insulator transition⁷⁹ takes place at this point, rather than at optimal doping, as reported earlier.

The present model suggests an attractive alternative interpretation for the QCP, as a *duality crossover* of the striped phase. (For other patterns of nanoscale phase separation, such as islands, this would correspond to a percolation crossover, but for 1D stripes, there is no true percolation.) At this doping, both magnetic and charged stripes have their minimum width, two cells. For lower doping, the magnetic cells widen, reducing coupling between the charged stripes, while for higher doping, it is the magnetic stripes that decouple. Correspondingly, below $x = 0.125$, there is a charge gap, leading to high-field localization, while above 0.125 there is a spin gap.

Note that this is not a conventional QCP, where there is an abrupt change of groundstate at $T=0$. For instance, for the 2D Hubbard model, on one side of the QCP there is believed to be a renormalized classical regime, with finite Néel order, and on the other side a quantum disordered regime, with a spin zero groundstate and a finite gap to the lowest triplet excitation. Instead, in the stripe crossover, magnetic layers persist on both sides of the duality crossover.

While both phases persist across the duality point, there is a crossover in the nature of the majority phase (magnetic or charged), and consequently the properties of the minority phase are strongly modified. Because of this, modifications need not occur exactly at the phase boundary. Instead, there strong changes in properties may be observed at any of a series of *magic dopings*, corresponding to the commensurate stripe phases discussed above.

For instance, the localization transition in LSCO occurs not exactly at $x=0.125$, but closer to 0.17. This could be understood as evidence that two-leg charged stripes are always localized, but 4-leg stripes are not. For a uniform stripe phase, the two-leg stripes would just disappear at $x = 2x_c/3 \simeq 0.167$. However, the localization behavior does not seem to be universal: in heavily underdoped YBCO, the resistivity of the normal state saturates at low temperatures, suggestive of a metallic state⁸⁰.

Again, the horizontal-vertical stripes are replaced by diagonal stripes at a doping 0.058, where the superconducting transition terminates. This is close to the doping of the (6,2) phase. (Note that the precise value of the magic dopings depends on x_0 ; the pure (6,2) phase

would fall at $x=0.058$ if $x_0 = 0.23$.)

Similarly, while there is not a conventional quantum disordered regime, a spin gap can still arise when the magnetic phase is the minority phase, although not necessarily at $x=0.125$. Indeed, in LSCO at $x=0.12$ there is well-defined long-range (incommensurate) Néel order³, with $T_N \simeq T_c$, the superconducting transition temperature. A simple interpretation of this result is that superconductivity is predominantly associated with the charged stripes, and the superconducting transition enhances charge phase stiffness, reducing the fluctuations of the charged stripes which were suppressing magnetic order on the magnetic stripes. At higher doping, the magnetic stripes are gradually spread apart, behaving more like two-leg ladders, and if the inter-ladder coupling becomes sufficiently weak, a spin gap can open up on each ladder. This is discussed further in Subsection VII.A.

Note that, while a duality crossover is a generic feature in a stripe model based on *phase separation*, there are alternative stripe models⁸¹ wherein the charged stripes are merely domain walls of antiferromagnetic domains, and a charge-stripe dominated regime would be meaningless.

VII. ISOLATED MAGNETIC STRIPE

In the stripe phase away from the duality crossover, the minority phase is present in the form of domain walls between domains of the majority phase. An important aspect of stripe phase theory is the development of a microscopic model for these domain walls. A number of groups have suggested a connection between magnetic stripes and even-leg ladders. Here, the magnetic domain walls in the higher-doping regime are modelled as two-leg ladders, which develop a spin gap as they move further apart, with reduced interladder coupling.

A. Spin Gap

In a stripe model, the magnetic neutron scattering near (π, π) should be reflective of the properties of the magnetic stripes. For LSCO, the incommensurability has been discussed above, Fig. 9, and is further discussed in the following subsection. In YBCO, incommensurability has only been resolved at one doping^{8,9}, but the doping dependence of the peak width is consistent with a similar underlying, but unresolved incommensurability¹⁰. In YBCO, the stripe model can also explain the doping dependence of the intensity of the magnetic neutron scattering near (π, π) , as well as the opening of a *spin gap*.

The doping dependence of the net intensity of the magnetic neutron scattering should reflect the relative density of magnetic stripes. For YBCO_{6+y}, the intensity was numerically integrated from Fig. 2 of Ref. 82, and the result plotted in Fig. 14. While the relation between y and hole doping x in YBCO is not completely settled, the

straight line illustrates a modified Tokura⁸³ expression, with the doping of the planes starting at $y = 0.2$, and varying linearly with y . The results are consistent with the picture that all magnetic scattering is associated with the magnetic stripes, and the stripe phase would terminate at an (inaccessible) doping $y = 1.095$. This would place the percolation crossover at $y \sim 0.65$, close to the plateau regime. Since the plateau has been interpreted as a $1/8$ effect^{84,15}, this suggests that the plateau doping is ~ 0.125 . This fixes the constant of proportionality: $x = 0.27(y - 0.2)$, so the charged stripe doping, corresponding to $y = 1.095$, would be ~ 0.25 , in excellent agreement with our other estimates. At optimal doping, $y \sim 0.925$, the hole doping would be ~ 0.2 . These estimates are also consistent with Tokura, et al.⁸³, who found $x = 0.125$ for $y = 0.75$, $x = 0.25$ for $y = 1$, and $x = .21$ for optimal doping. The inset to the figure shows that $T_c(x)$ follows the familiar parabolic form⁸⁵,

$$\frac{T_c}{T_{c,max}} = 1 - \left(\frac{x - x_m}{x_w}\right)^2, \quad (10)$$

with $T_{c,max} = 92K$, $x_m = 0.2$, and $x_w = 0.16$. Note that the dip in T_c near the 60K plateau is close to $x = 1/8$.

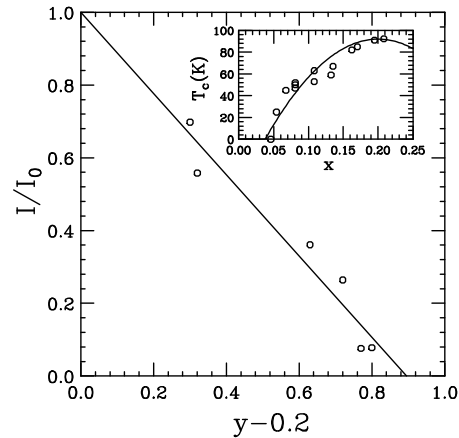


FIG. 14. Intensity of magnetic scattering vs. doping for YBCO. Circles = data of Ref.⁸²; line = expected result for stripe model.

The falloff of intensity is likely to be even steeper than illustrated in Fig. 14, since the data were presented only up to about 60meV, while at the lower doping levels, there is considerable intensity at higher frequencies.

The spectrum of the excitations near (π, π) has a complicated evolution with doping, and below the superconducting T_c , the intensity is suppressed below a doping dependent energy, called the ‘spin gap’⁸². This gap is distinct from the pseudogap, and has a strikingly different doping dependence, Fig. 15. A similar gap is seen in LSCO^{86,87}, but so far only near $x = 0.15$. There it is found that the spin gap is isotropic⁸⁷, further evidence that it is distinct from superconductivity or the pseudogap.

The doping dependence of this spin gap in YBCO can be interpreted simply in terms of coupled magnetic ladders, Fig. 15. Below the $1/8$ crossover, the magnetic stripe (ladder) width decreases smoothly with doping, while the interladder coupling is approximately constant, since the hole-doped stripe has fixed width. Theoretically, the spin gap is found to be (approximately) inversely proportional to the ladder width⁸⁸, so in this regime the spin gap scales linearly with doping, $\Delta_s = \beta J/M$, where J is the exchange constant, M the ladder width, and β a correction for interladder coupling, $\beta \simeq (1 - 4J''/J)$, with J'' the exchange coupling between adjacent ladders⁸⁹. The solid line in Fig. 15 corresponds to $J'' = 0.21J$.

Above the crossover, $x > x_0/2 = 0.125$, M is fixed at 2 while β increases with doping, since J'' decreases as the hole-doped stripes widen. Since the Cu in the hole-doped stripes can be magnetized, the falloff should be relatively slow. Details are model sensitive, but qualitatively the observed behavior is readily reproduced. The curve in Fig. 15 follows from assuming a falloff $J'' \sim N^{-1}$, where N is the hole-doped stripe width, inset to Fig. 15. (It should be noted that the falloff is sensitive to the hole-density x_0 , here taken as 0.25.)

The model predicts⁸⁹ that for an isolated stripe, the spin gap equals $J/2$, at least when the exchange constant is the same on all rungs and links. From Fig. 15, this implies a limiting value $J \sim 80\text{meV}$ at $x = 0.25$, considerably smaller than the $x = 0$ value $J = 130\text{meV}$. Such a doping dependence for J is not unexpected. For simplicity, however, the model assumes a constant value for J ; this value must be taken as $J = 80\text{meV}$, to successfully model the single stripe limit. The value is less critical near zero doping, where the gap is small.

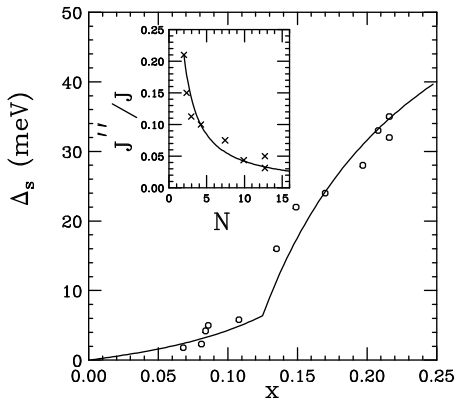


FIG. 15. Spin gap Δ_s vs. doping for YBCO. Circles = data of Ref.⁸²; line = theory, assuming solid line from inset. Inset: interladder exchange vs. hole-doped stripe width.

In this model, the spin gap should already exist in the normal state. The striking change observed at T_c can be explained as a fluctuation effect, similar to those seen in the BSCCO photoemission. Strong fluctuations at high temperatures prevent any long-range stripe or-

der or true spin gap. The superconducting transition leads to three-dimensional coherence, and hence greatly suppresses charge and spin fluctuations in the stripes. Hence, a long range spin gap can open on the magnetic stripes below T_c . Consistent with this interpretation, it should be noted that the spectrum in the normal state in heavily doped YBCO has been interpreted^{90,87} in terms of a formula derived for spin-1 chains⁹¹, and hence expected to approximately hold for spin $1/2$, 2-leg ladders.

B. Incommensurability Saturation

Inelastic magnetic neutron diffraction finds a saturation of the incommensurability in LSCO at approximately $x = 1/8$. Within the present framework, there are actually several possible explanations for the saturation. One was discussed above, Fig. 9: strong Coulomb interactions arrest the phase separation at the (2,2) stripe, and higher doping causes these stripes to gradually fill in.

On this interpretation, the Coulomb effects are much stronger in LSCO than in YBCO, and the isolated spin gap regime (right-hand side of Fig. 15) would not exist in LSCO. The Coulomb effects would indeed be expected to be stronger in LSCO, since interlayer screening is weaker. In Nd-substituted LSCO, due to the LTT phase structural distortions, stripes in alternate layers are rotated by 90° ; a similar situation may arise in LSCO, perhaps due to LTT fluctuations. On the other hand, in YBCO the magnetic correlations have a strong c -axis modulation, suggesting that stripes in both CuO_2 planes of a bilayer run parallel, with the charged stripes offset laterally to provide stronger interlayer screening.

However, there are other plausible explanations for incommensurability saturation. Even before the discovery of stripes, it was found that LTO and LTT domains of fairly large size (producing distinguishable diffraction peaks) coexist near $1/8$ doping in LBCO. It seems plausible that this is associated with a stripe commensurability effect, similar to that found in the nickelates, and that a similar effect arises, at least incipiently in LSCO. In this case, the residual magnetic scattering would be due to regions that have not yet been doped beyond $1/8$. In the more highly doped domains, the magnetic stripes would have a spin gap: since the ground state of a two-leg ladder is a spin singlet, it does not contribute to the magnetic scattering. A related problem has been studied by Kim, et al.⁹², who showed that in a random mix of weakly coupled three-leg (magnetic) ladders and two-legged (spin-gapped, and hence non-magnetic) ladders, the magnetic incommensurability remains unchanged from that of the pure array of three-legged ladders.

Even without commensurability effects, one would expect $1/8$ lock-in over a finite doping range, when the 2,2 stripes coexist with 2,4 stripes, which have a well defined spin gap. In this case, the magnetic incommensurability should be fixed at that for $1/8$ throughout the

coexistence regime, but should disappear when a commensurate 2,4 phase is stable, at $x = 2x_0/3 \simeq 0.17$. In LSCO, the 1/8 stripes are actually found^{1,2} to persist up to $x \simeq 0.25$. Hence the need to postulate lock-in effects at 1/8 doping, the exact analog of the stability of the $x = 1/3$ and 1/2 striped phases in nickelates. In this case, the heavily doped phases would have no magnetic scattering, while the 1/8 stripes would have a scattering of fixed incommensurability, but decreasing intensity and increasing width, as the stripe domains shrink in size. The special stability of the 1/8 phase may be associated with the finite residual exchange coupling across the two-cell-wide charged stripes, which is responsible for the antiphase boundaries, and which may be lost in wider charged stripes, or with the reduced Coulomb energy.

At this stage, there is not enough information to judge between the two models for incommensurability saturation. The former, strong Coulomb effect, has the advantage that it could simultaneously explain why T_c in LSCO is so low – the local hole density is forced away from optimal. However, there is considerable evidence that stripe phase order is better developed in LSCO than in other cuprates, and this could provide reason enough for a lower T_c .

In many ways, optimally doped LSCO resembles an underdoped YBCO. We have here suggested that this is because stripes and pseudogaps in both materials persist up to $x \simeq 0.25$, whereas T_c is optimal near 0.16 in LSCO, 0.2 in YBCO. Sato, et al.⁹³ have recently provided additional evidence that the pseudogap opens well above T_c in optimally doped LSCO.

VIII. DISCUSSION

A. Improvements for the Stripe Model

The present model of the stripe phase provides a significant advance over earlier calculations. In these early calculations, an external stripe potential was imposed, which could be either periodic or random, and the rearrangement of holes was studied. It was found that the stripes produced minigaps, but that an average, smeared dispersion and Fermi surface could still be defined. However, there was no sign of the split dispersion (magnetic vs charged stripe) found in photoemission experiments. The present calculation replaces the external potential with a given, doping dependent potential, and studies how holes redistribute in the presence of a competition between that potential, which favors phase separation, and Coulomb repulsion, which favors a uniform density distribution. The striking result is that the resulting dispersion resembles a weighted superposition of the dispersions of the two end phases, with the addition of some superlattice minigaps. This is very encouraging, in providing an explanation for the photoemission results. Moreover, it shows that the mechanisms responsible for the

special stability of the end phases can continue to operate on these nanoscopic length scales.

A number of improvements still need to be made in the model. The next step would be to make the calculation fully self-consistent, by eliminating any assumed potential, and directly calculating and minimizing the free energy of the striped phase. Since the dispersion is not greatly changed, it is unlikely that this additional step will greatly modify the present results. The most likely change would be that the densities could adjust slightly to take advantage of the minigaps, better centering them at the Fermi level. This could lead to a more systematic growth of the pseudogap with underdoping, since the minigaps are associated with the charged stripes, and get larger as these stripes get narrower. The idea that the pseudogap is associated with stripe minigaps has been proposed previously⁹⁴; the present calculation provides a systematic doping dependence and a connection with the VHS.

A complete understanding of the stripe phase, particularly in BSCCO, lies in the correct inclusion of fluctuation effects. These effects can broadly be separated into two categories, depending on whether the fluctuation preserves the local density distribution or not. In the former category fall fluctuations in the local stripe spacing, either static or slowly varying in time, and long-wavelength bending of the stripes. It is likely that the energy dispersion is a fairly localized function in space, and that these fluctuations can be calculated as weighted averages over the present solutions. In this case, the dispersion would still be a superposition of the two end phases, and the main effect of the fluctuations would be to smear out the minigaps. Since there is always a gap near the Fermi level, a residual pseudogap should survive. Moreover, since the split-off LHB is well defined, particularly at lower doping, it should persist at a distinguishable feature after averaging. This would resemble the photoemission in LSCO.

The second class of fluctuations involves fluctuations which are fast enough, or disordered on a sufficiently short-wavelength scale so that the local density does not lie near the two potential minima. These fluctuations act to wipe out the stripe fluctuations on a local level, and the question is, can they describe the experimental results in BSCCO, where, for $T > T_c$, the two valence bands appear to collapse into a single reconstructed band. This is a plausible result: as a line of holes fluctuates back and forth in an antiferromagnetic background, the background will have to adjust to some time-averaged hole density. The theoretical problem is how to properly include this averaging; it is a question of how the system responds locally on different time scales.

B. Four Types of Gap

It should be noted that the present model has four distinct types of gap in the electronic spectra. First, there is the Mott-Hubbard gap in the magnetic stripes, e.g., Fig. 7a. Then there is the Van Hove gap on the charged stripes, Fig. 10. It is postulated that the opening of these two gaps provides the stabilization energy of the stripe phase, as in Fig. 2. However, in addition there is a third type of gap, arising from the new periodicity associated with the stripe phase. This leads to minigaps in the dispersion across the stripes, clearly visible in Fig. 7b-d. Finally, there is the superconducting gap.

Many earlier discussions of the pseudogap relied on the photoemission studies of BSCCO in the *normal* state. The recent systematic studies in BSCCO^{68,69} and LSCO⁶⁶ suggest that the low-temperature data are more representative of the stripe phase. In this case, Fig. 13 shows that there are two distinct features, and the Mott-Hubbard gap is associated with the ‘hump’ feature in BSCCO; the ‘peak’ feature is then plausibly associated with the charged stripes. The question then is which of the remaining three theoretical gap features accounts for the ‘peak’.

The doping dependence of the peak feature is not consistent with a conventional superconducting gap: the transition temperature T_c decreases while the peak energy Δ_p increases with increasing underdoping. It has been suggested⁹⁵ that Δ_p is superconductivity-related, but associated with preformed pairs. However, in the case of a multicomponent order parameter, it has been shown that the total gap at $(\pi, 0)$ is a vector sum of the individual components. In BSCCO, a careful analysis of the data⁹⁶ (involving the detailed doping dependence of the ‘dip’ feature) suggests that the gap is best interpreted as a superposition of a superconducting component and a non-superconducting component, with the latter dominating in the strongly underdoped limit. Accepting this analysis, the question becomes, what is the origin of the non-superconducting component on the charged stripes?

The experimental observation that this peak increases as the hole doping decreases cannot be easily explained in terms of conventional Van Hove gaps, which are largest at x_0 , Figs. 2 and 11. A model involving Van Hove pinning, introduced⁴⁶ to explain the pseudogap crossover in BSCCO, relied on the normal-state data, which appeared to show a smooth evolution into the magnetic stripe at half filling. The model cannot explain the evolution of a distinct charge-stripe gap.

On the other hand, the minigaps seen in Fig. 7 do on average grow larger as the doping is reduced, saturating near the 1/8 crossover. In the present, non-self-consistent calculation, these minigaps are not centered on the Fermi level. However, it is clear that having E_F fall in a minigap would enhance the energy lowering, stabilizing these gapped phases and improving agreement with experiment. It should be noted that the greatest

energy lowering would correspond to having E_F centered on the minigap closest to the VHS, since that is where the dos is highest, Fig. 16. This would then be a form of *stripe-induced Van Hove splitting*.

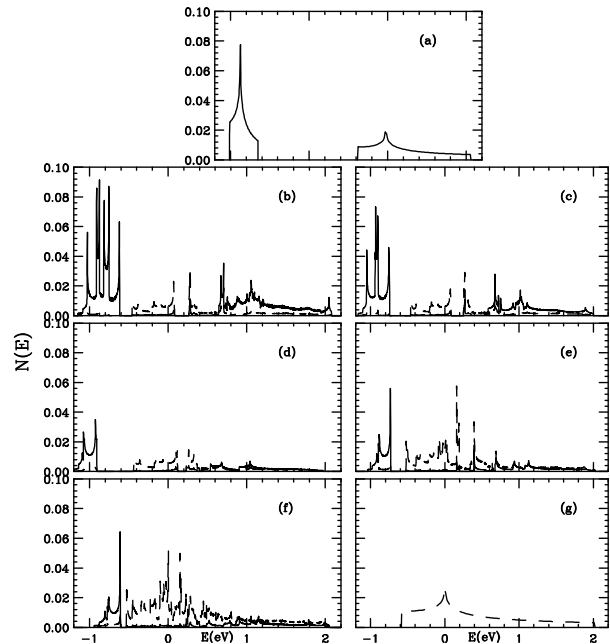


FIG. 16. Density of states for dopings: $x = 0$ (a), 0.0625 (b), 0.0833 (c), 0.125 (d), 0.167 (e), 0.1875 (f), and 0.25 (g) assuming dielectric constant $\epsilon = 15$. (The $x = 0$ data are shifted up by 0.16eV.) Solid (dashed) line = partial density of states for magnetic (charged) stripes.

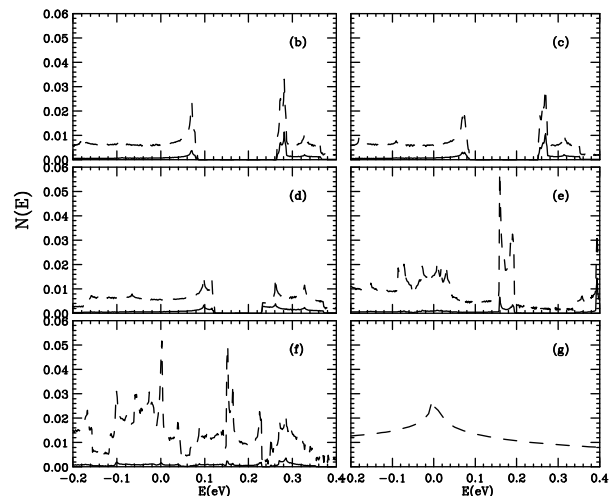


FIG. 17. Blowup of density of states near E_F , for same dopings as in Figure 16. (There is no frame (a), since the dos vanishes in this energy regime.)

Note that the largest minigap is associated with this VHS splitting, even in the lowest doping situation, (6,2).

Figure 17 shows a blowup of the dos near the Fermi level. It can be seen that there is a gap (dos = 0) for $x \leq 0.125$, centered at an energy $\sim 0.18eV$ above E_f . For larger x a pseudogap (dos > 0) persists, shifting toward E_f with increasing doping. Since the problem is two dimensional and the stripes are fluctuating, this gap will be spread out into a pseudogap. Nevertheless, the low dos means that localization effects should be present. Since the (pseudo)gap remains large at the 1/8 crossover, there should be a delocalization transition at a somewhat higher doping. In the present calculation, this feature falls above the Fermi level; however, this could change in a fully self consistent calculation.

Finally, one should note the duality between the charge stripe minigap, which grows as hole doping is reduced, Fig. 13, and the magnetic stripe spin gap, which increases with increasing hole doping, Fig. 15.

C. Fermi Surface and Remnant Fermi Surface

Figure 18 shows the Fermi surfaces corresponding to the same dopings as in Fig. 7. As expected from the ‘projected’ dispersions in that Figure, in all cases the wave functions are > 90% associated with the charged stripes. Note the important role of the structure factors: while there is a well-defined superlattice in each case, and hence each Fermi surface segment is periodically repeated, the weight is highly nonuniformly distributed, being concentrated predominantly near the limiting $x=0.25$ Fermi surface (solid line in the figures).

Feng, et al.⁹⁷ recently presented photoemission evidence for the presence of *two* Fermi surfaces in BSCCO, seen at different incident photon energies. This result is disputed⁹⁸, but it is intriguing that the ‘new’ Fermi surface has large flat sections, very similar to the 1/8 stripe pattern, Fig. 18b.

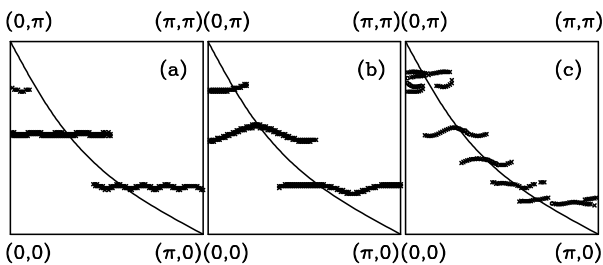


FIG. 18. Fermi Surfaces for dopings: $x = 0.0625$ (a), 0.125 (b), and 0.1875 (c), and $\epsilon = 15$. Solid line in each is the Fermi surface for $x=0.25$.

Ronning, et al.⁵⁸ introduced an alternative, well-defined energy surface, which they refer to as a ‘remnant Fermi surface’ (rFs). This is the locus of points where the integrated photoemission intensity, taken as proportional to $n(k)$, falls to one half its maximal value. While the intensity does fall to half at the Fermi level, it can also

fall to half at an energy away from the Fermi level (N.B., the rFs is not a surface of constant energy). Indeed, a rFs was found for the insulating CCO. We have shown that in this case the rFs (the locus of points where the coherence factor equals one half) maps out the superlattice zone boundary. (Since the model does not include fluctuations, there is only one band below E_f , and hence no photoemission distribution to integrate over.)

In the case of a stripe array, there are several complications. First, there are several subbands, and one will get different results depending on whether one calculates an rFs for each subband, or a single rFs for the whole valence band. The structure factor provides an additional complication, since the intensity is almost never the full possible value. Nevertheless, for simplicity, Fig. 19 plots the locus of points where the net spectral function equals $1/2$ – actually, falls within a range 0.48-0.52. Comparison of Figures 18 and 19 shows that the true Fermi surface and the rFs are quite distinct features, and that the rFs tends to follow the superlattice Brillouin zone boundaries.

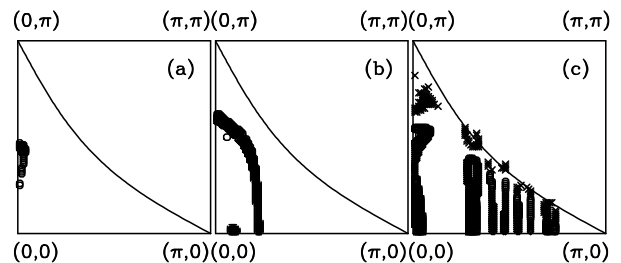


FIG. 19. Remnant Fermi Surfaces for same dopings as in Fig. 18: $x = 0.0625$ (a), 0.125 (b), and 0.1875 (c).

D. Staging

A test case for phase separation models of stripe formation comes from measurements on oxygen-doped $\text{La}_2\text{CuO}_{4+\delta}$. In these materials, the interstitial oxygens are highly mobile, so the tendency of holes to phase separate leads to *macroscopic* phase separation. As in graphite intercalation compounds (GIC), this is accomplished by staging⁹⁹: the interstitial oxygens form dense layers, with subsequent oxygen layers separated by n layers of CuO_2 (n is the stage number). The puzzling observation⁵ is that despite the macroscopic phase separation, stripes are still found in these compounds. I suggest the following resolution, also based on an analogy with GIC. The stripes were observed in a predominantly stage 4 compound, with 4 CuO_2 layers per oxygen interstitial layer. In GIC, a stage 4 would have a highly inhomogeneous charge distribution, with most of the charge on the bounding layers (in this case, the CuO_2 layers adjacent to the interstitial O’s), and significantly less on the interior layers, away from the O’s. Hence, in the cuprate I propose a similar effect: fully charged $x \simeq 0.25$ bounding layers, and lighter charged $\sim 1/8$ interior layers.

Thus, the staging is driven by the tendency to phase separate, producing ideal hole-doped bounding layers, but there are still stripes due to doping of the interior layer. This model resolves two additional problems. First, the sample was a mixture of stages 2 and 4. If the doped holes were uniformly distributed on all CuO_2 layers, then there would be *two independent stripe patterns*, since the stage 2 CuO_2 planes would have nearly twice as many holes per layer. Within the present model, most of the charge goes into the bounding layer, so the layers of stage 2 would have comparable doping to the bounding layers of stage 4; moreover, since both types of layers are nearly fully doped, neither would show magnetic scattering.

Finally, even though static stripe order was observed, there was no reduction in T_c – indeed, $T_c=42\text{K}$ is higher than can be obtained with Sr doping. This can most easily be understood if the superconductivity and the stripe order are in different layers.

E. Comparisons with Slave Boson Results

It is instructive to compare the present results with earlier slave boson calculations. In the simplest version, there is no magnetic coupling, $J = 0$, and the band structure near the Mott transition is highly anomalous. There is a single band, but as the doping approaches half filling, $x \rightarrow 0^+$, the bandwidth vanishes, with both t and t' renormalized to zero. In the three-band model, even after setting $U \rightarrow \infty$, there is still a charge transfer energy, Δ . In this case, it is also possible to approach half filling from below, $x \rightarrow 0^-$; the same bandwidth collapse occurs, but at a different energy, E^- , with $E^- - E^+$ being the (renormalized) charge transfer energy.

Is there any way to reconcile the present results with slave boson theory? I suggest the following possibility. When a hole is doped into the Mott insulator, there is phase separation, and locally the dispersion is restored: $t \rightarrow t_0$. At a doping x , a fraction x/x_0 of the electrons have hopping $\sim t$, the rest ~ 0 . But in the mean-field slave boson calculation the effect of the hole is uniformly spread out over the entire lattice, leading to an effective $t \rightarrow xt_0$. This is just what is found in the present stripe calculation. As the material is doped, the magnetic band persists with little change, while a new band appears, characteristic of the hole-doped stripes, with full bandwidth, $t \sim t_0$ (neglecting superlattice gaps), but with relative intensity proportional to x , Fig. 7. If this interpretation is correct, it suggests that the slave boson calculation may underestimate the tendency for phase separation.

F. Comparisons with Other Calculations

A number of calculations^{100,101,46} interpret the magnetic stripe dispersion in terms of a flux phase rather than an antiferromagnet. This is unsatisfactory for two reasons: first, there is clear evidence that the magnetic stripes have predominantly antiferromagnetic correlations; and secondly, the flux phase has zero gap at $(\pi/2, \pi/2)$, making it difficult to explain the dispersion in SCOC, which has a gap $\geq 0.8eV$. The present calculation is based on an antiferromagnetic model, which corrects both of these defects.

The dispersion in the presence of stripes has also been calculated by SEK²⁰ and by Seibold, et al.²¹. These calculations were intended simply to show the effect of charge (or spin) modulations on the quasiparticle dispersion and involve highly simplified models for stripes. SEK introduced a background stripe potential, $V_\sigma(\vec{R})$, which fixed the orientation and periodicity of the stripe array, and induced a modulation in the quasiparticle charge and spin densities. Seibold, et al. concentrate on the charge modulation, and introduce a CDW model, again with externally imposed periodicity.

While these calculations demonstrated how the modulation introduces pseudogaps into the dispersion, they are not expected to give a very good picture of stripes arising from an underlying phase separation instability. A CDW model involves a *fixed periodicity* and a *variable density*, whereas phase separation should produce an approximately fixed density and smoothly varying periodicity. Thus, in the present calculations, it is straightforward to model the full doping dependence of the stripe phase; in the earlier calculations, the doping dependence of the periodicity and potential must be supplied empirically, so the models can make no predictions. Thus, neither calculation showed any sign of the separate magnetic and charge bands.

One should note a distinction between the way the idea of CDW's is applied in these calculations and the usage of the present paper. In the earlier calculations^{20,21}, the charge modulation of the stripes *is* the CDW. In contrast, the present paper envisages CDW's (or related phonon anomalies, such as the LTT phase) as existing on the charged stripes, leading to two inequivalent sublattices – much as antiferromagnetism leads to two sublattices on the magnetic stripes.

In a recent paper, Pryadko, et al.¹⁰² presented a detailed criticism of the early Hartree-Fock calculations of stripes. In these calculations, the stripes are claimed to arise from Fermi surface nesting, so some of the criticisms apply to a larger class of models. Here, I would like to take issue with some of the statements. First, Pryadko, et al. state “the density of holes along a stripe varies continuously as a function of x ”, citing Yamada, et al.². While this is mainly associated with the saturation of the incommensurability above $x=1/8$, they note that the data at lower doping also show some curvature,

suggestive of a ‘slight variation’ of the doping. This is mainly associated with the cutoff of incommensurability below $x \simeq 0.06$, but that data have now been superseded by better samples: the stripes are present, but rotated by 45° , and the incommensurability falls close to the Yamada (straight) line. As discussed above, both a slight doping-dependence below $x = 1/8$, and a stronger saturation above that doping *can* be understood in a model with a preferred charged stripe density, in the presence of either long-range Coulomb repulsion (which can produce a *real* saturation of the incommensurability) or commensurability pinning (which produces an *apparent* saturation).

Pryadko, et al. further state, “In the LSCO family, ..., there is simply no vestige of a quasiparticle in the region of momentum space where the nested Fermi surface is supposed to occur.” This statement raises several issues. First, one must carefully distinguish conventional Fermi surface nesting from Van Hove nesting. For the conventional nesting model¹⁰³ they cite, the nesting is associated with flat sections of Fermi surface; in LSCO these flat sections arise near¹⁰⁴ $(\pi/2, \pi/2)$, where there *are* well-defined quasiparticles. Conversely, the fact that these quasiparticles persist in the striped phase shows that they are not involved in the nesting process.

In contrast, in Van Hove nesting the important quasiparticles are those near $(\pi, 0)$. In all the cuprates, these quasiparticles are found to be shifted below the Fermi level, and indeed *a comparison of photoemission and tunneling studies reveals that the position of these quasiparticles defines the pseudogap* – exactly as required by a Van Hove nesting theory. Moreover, even in the SEK calculation it was clear that these Van Hove quasiparticles, which constitute the ‘flat bands’ remain well defined in the calculated striped phase. This is further clear from, e.g., Fig. 7 above. True the quasiparticles are greatly smeared out, but this is a direct consequence of the formation of stripes, and cannot be taken as an argument against this mechanism of stripe formation.

Finally, Stojković and Pines¹⁰⁵ claimed to rule out the VHS in the physics of the cuprates. They employed parameters for which the VHS falls at very high doping, $x = 0.55$, and concluded “the presence of the van Hove singularities near the Fermi surface plays only a marginal role”. However, their more recent calculations⁵⁴ employ a revised parameter set (i.e., $t' = -0.25t$), which places the VHS at $x = 0.22$, close to the present $x_0 = 0.25$.

IX. CONCLUSIONS

This has been a long manuscript, which presents a coherent view of the stripe phases in the cuprates. A number of principal results of the calculations are here summarized. Most of the results are *generic*, and would be expected in any model where the stripes result from two-phase coexistence, while a few are specific to a Van

Hove scenario.

(1) This is the first calculation of photoemission in the stripe phase involving strong stripe correlations, i.e., preferred hole dopings with independent characteristic dispersions, as opposed to a single dispersion with sinusoidal (CDW/SDW) modulations.

(2) This allows a study of the evolution of the dispersion as a function of hole doping.

(3) It is found that, even at this nanoscale level, the dispersion can be characterized as a *superposition of two components*, leading to a picture of magnetic stripe bands and hole-doped (‘charged’) stripe bands. This allows a natural interpretation of the photoemission spectra in LSCO, and suggests a unified picture with BSCCO and SCOC.

(4) The calculations suggest that an important role of the superconducting transition is to freeze out fluctuations of the stripes. This freezeout manifests itself in three ways: (a) the electron-electron scattering rate drops by several orders of magnitude below T_c ⁷¹; (b) the photoemission dispersion splits in BSCCO into a characteristic peak-dip-hump structure; (c) the (π, π) magnetic neutron scattering in YBCO sharpens below T_c , revealing a characteristic spin gap.

(5) The doping dependence naturally leads to a picture of a series of *quantum critical points* (QCP’s) or magic dopings, at which the stripe pattern is commensurate with the crystalline lattice. The most prominent one is the famous 1/8 effect, but the metal-insulator transition in LSCO and the onset of superconductivity are close to two other magic numbers.

(6) The percolation crossover at 1/8 doping provides a simple model of the spin gap in YBCO, showing that a two-leg ladder provides a good model for an isolated magnetic stripe.

(7) As a result of point (3), the model has a *natural VHS pinning* to the Fermi level: if the VHS is at the Fermi level in the charged stripe end phase (as it must be, if this phase is stabilized by Van Hove nesting), then the VHS remains close to E_F over the entire doping range.

(8) This provides a new explanation of the pseudogap: *stripe-induced Van Hove splitting*.

(9) More speculatively, since superconductivity in YBCO is strongest well beyond the percolation crossover (1/8 effect), *superconductivity seems to be a property predominantly of the charged stripes*.

There are a number of advantages of the present model of fractionally-doped stripes. First, if the stripes are stabilized by CDW formation, then there is an important continuity between stripes in the cuprates, and those in the nickelates and manganites. Such continuity is lost in the SO(5) model, where the charged stripes are stabilized by superconductivity. Moreover, a connection with CDW’s would naturally explain the experimental observation that the stripe phases are dominated by charge order rather than spin order, a result difficult to understand in a pure Hubbard or tJ model.

Acknowledgment: These computations were carried

out using the facilities of the Advanced Scientific Computation Center at Northestern University. Their support is gratefully acknowledged. I thank C. Kusko, S. Sridhar, A. Bansil, B. Barbellini, and M. Lindros for stimulating conversations. Publication 776 of the Barnett Institute.

APPENDIX A: WHITE-SCALAPINO STRIPES

It remains an open question whether phase separation is a generic feature of the Hubbard and tJ models, or arises only in a restricted parameter domain. In the tJ model, the recent density-matrix renormalization group (DMRG) calculations of White and Scalapino (WS)^{40,41} find clear evidence for stripes, but even these results are controversial: some groups find that stripes are metastable within the tJ model^{106,107} (see the discussion in Refs. 108,109), others that the model should display macroscopic phase separation¹¹⁰. Moreover, inclusion of realistic values of t' into the model further reduces the stripe stability^{111,112}. Nevertheless, they represent at worst a low-lying excited state, and hence may become the true ground state in the presence of additional interactions (e.g., electron-phonon coupling).

It is interesting to note that many of the DMRG results can be simply understood in terms of a phase separation model. This hypothesis can explain four quantitative results of WS: (1) At 1/8 doping, WS⁴⁰ find hole-doped stripes which are 2 Cu atoms wide, with doping ~ 0.25 holes per Cu, which they interpret as a bond-centered domain wall with 0.5 holes per unit length. Increasing the doping, (2) they find a remarkable transition to stripes with 1 hole per unit length⁴¹, (3) which coexist with the 0.5 hole stripes for $0.125 \leq x < 0.17$, and finally, (4) the stripe phase disappears at $x=0.3$.

All of the above features can be simply understood by assuming that the hole-doped stripes have a density $x^* \sim 0.25$ hole/Cu, and that there is a preference for both magnetic and charged stripes to have even width. Hence, the narrowest possible magnetic stripes are two cells wide.

Given these assumptions, the WS data can be explained as follows. In the low doping regime, hole doped stripes form with the minimal width of two cells, and 0.25 holes per Cu, for a net of 0.5 holes per unit length. This continues up to 1/8 doping, at which point both magnetic and hole-doped stripes are two cells wide. Doping holes beyond 1/8 doping can be accomplished by increasing the width of the hole-doped stripes. A stripe 4 Cu wide has $4 \times 0.25 = 1$ hole per unit length. The sample will be a mix of 2-Cu and 4-Cu stripes until $x = 2x^*/3 \sim 0.167$, and when $x = x^* \sim 0.25$, the whole sample is filled with the hole-doped phase, and the stripe phase terminates. This last number is lower than the simulation, $x = 0.3$, and may be evidence that x^* is weakly doping dependent.

The WS simulations actually display this increase in stripe width above 1/8 doping, Fig. 4a of Ref.⁴¹. This is

more clearly seen in plots of the rung-averaged hole density, Fig. 20. The data (open circles) fall very close to the form expected for a phase separation model (solid lines), with the same average densities as at 1/8 filling, but now the magnetic stripes retain their minimum width, while the hole-doped stripes get wider.

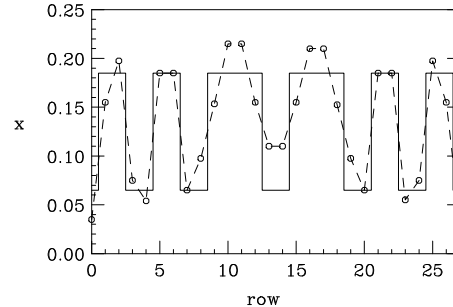


FIG. 20. Rung-averaged hole density (open circles)⁴¹, interpreted as constant hole density domains of variable width. Dashed lines = guides to the eye; solid lines = phase separation model.

It should be stressed that the mechanism responsible for stabilizing the WS stripes is unknown, but clearly does not involve the VHS, being weakened by a finite t' . Even should the WS stripes prove to be the ground state, it may still be that they are too weakly bound to explain experimental observations. The debate on their stability suggests that non-striped phases lie very close in energy – for instance, Hellberg and Manousakis¹⁰⁹ find energy differences of the order of 1meV. But it is found that the stripe phase separation collapses when the temperature becomes comparable to the energy barrier between the phases¹¹³, Fig. 21.

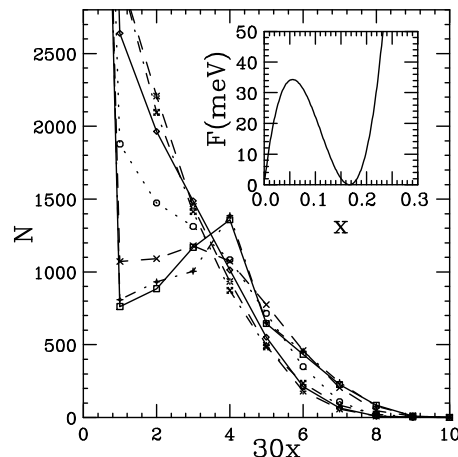


FIG. 21. Striped phase melting transition at $x=0.04$, $\epsilon = 23$: hole distribution function at temperatures (reading from bottom to top, at fixed hole occupancy $30x = 2$) $k_B T = 10, 0.1, 30, 60, 100, 400, 200$ meV. Inset: Assumed free energy vs. doping.

It should be noted that Figure 2 of Ref. 113 was printed incorrectly in the original publication. The correct figure is included here, as Fig. 21. The calculations are described in the original publication. Note that, at low temperatures, the particle distribution is two peaked, corresponding to the two kinds of stripes, while at high temperatures the distribution collapses into a monotonic limit. The crossover temperature scales with the free energy barrier between the two phases.

APPENDIX B: MORE ON THE SDW DISPERSION

As will be shown below, the SDW model gives a surprisingly good description of the photoemission dispersion, not only in the insulating limit, but also in doped BSCCO. However, if M is interpreted as the long-range Néel order parameter, there are problems with the doping dependence, Fig. 1, and the temperature dependence, Fig. 22. On the other hand, since this is a mean-field calculation, it is more plausible to interpret M as a measure of short-range antiferromagnetic order, and the transition as describing the splitting of the upper and lower Hubbard bands. To stress this point, the transition is labelled as T_H . Figure 22 shows the temperature dependence of the magnetization, while the inset shows the dependence of T_H on U/t . These results are consistent with the three-dimensional calculations of Dichtel, et al.⁶¹

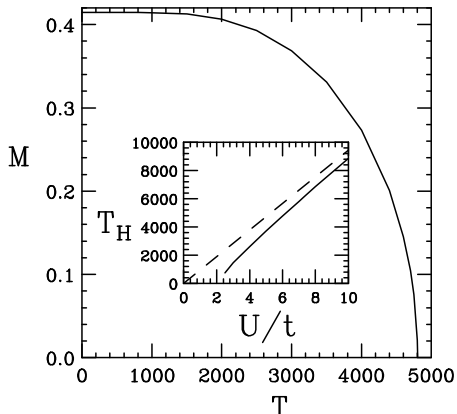


FIG. 22. Temperature dependence of magnetization in mean-field model. Inset: U -dependence of T_H . Dashed line: $T = U/4$.

Interpreting the doping dependence of M as a measure of the renormalization of the *splitting* into upper and lower Hubbard bands, the mean-field calculations are in good agreement with exact diagonalization calculations⁶² and experiments on the cuprates⁶³.

Figures 23-26 show how the dispersion changes with doping. For all curves, the same band parameters, given below Eq. 4, are used, with $M(x)$ found self consistently. Surprisingly, the results are qualitatively consistent

with the pseudogap in the underdoped cuprates (\times 's, diamonds, and squares)^{114,68}, even though no striped phases are assumed. However, the predicted hole doping is anomalously large.

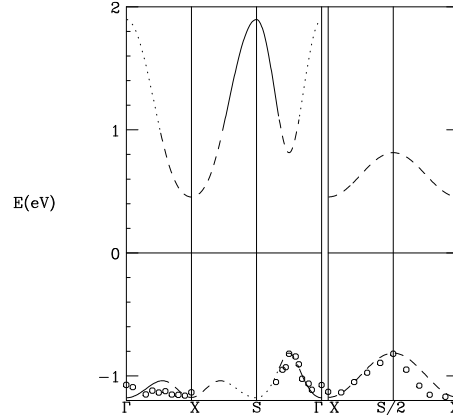


FIG. 23. Dispersion of the antiferromagnetic insulator in mean-field model. Open circles = data of Ref.⁵⁷. Solid lines: coherence factor > 0.8 ; dashed lines: $0.8 >$ coherence factor > 0.2 ; dotted lines: coherence factor < 0.2 .

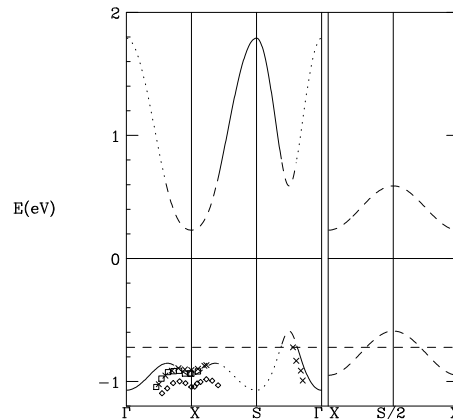


FIG. 24. Dispersion of the doped antiferromagnet, $x = 0.169$, in mean-field model. \times 's = data of Ref.¹¹⁴ (underdoped, $T_c = 67K$); diamonds (underdoped, $T_c = 52K$) and squares (overdoped, $T_c = 72K$) = data of Ref.⁶⁸; solid lines: coherence factor > 0.8 ; dashed lines: $0.8 >$ coherence factor > 0.2 ; dotted lines: coherence factor < 0.2 . Horizontal dashed line = Fermi level.

In the undoped material, the model has a direct (indirect) Mott-Hubbard gap of 1.63eV (1.27eV), and reproduces the dispersion found in the oxycuprates^{57,58}, Fig. 23. Here $X = (\pi, 0)$, $S = (\pi, \pi)$, and $\bar{S} = S/2$. The spectral weight is proportional to the coherence factor

$$\zeta_{\pm} = \frac{1}{2} \left(1 \pm \frac{\epsilon_{-}}{W} \right), \quad (\text{B1})$$

with the subscript $+$ ($-$) referring to the upper (lower) Hubbard band. From Fig. 23 it can be seen that the

coherence factor is ≤ 0.5 all along the $X \rightarrow S$ branch, where no quasiparticle peaks were reported. The weight along the line $X \rightarrow \bar{S}$ is uniformly $1/2$, characteristic of the antiferromagnetic zone boundary^{52,115}.

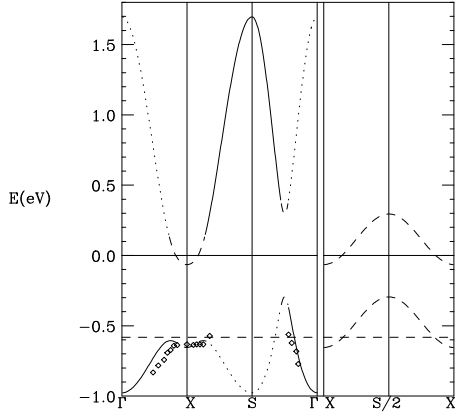


FIG. 25. Dispersion of the doped antiferromagnet, $x = 0.356$, in mean-field model. Diamonds = data of Ref.¹¹⁴ (overdoped, $T_c = 85K$); solid lines: coherence factor > 0.8 ; dashed lines: $0.8 >$ coherence factor > 0.2 ; dotted lines: coherence factor < 0.2 . Horizontal dashed line = Fermi level.

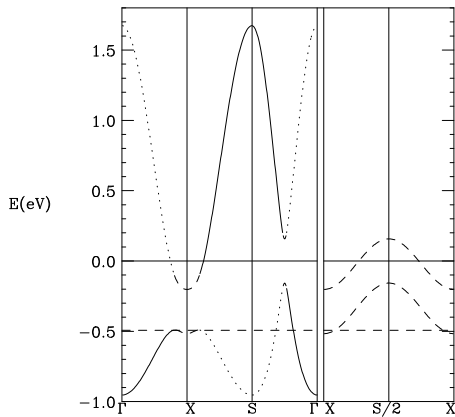


FIG. 26. Dispersion of the doped antiferromagnet, $x = 0.392$, in mean-field model. Solid lines: coherence factor > 0.8 ; dashed lines: $0.8 >$ coherence factor > 0.2 ; dotted lines: coherence factor < 0.2 . Horizontal dashed line = Fermi level.

In studies of the Fermi surfaces of the hole-doped cuprates, there is an important question as to whether the Fermi surfaces are large, centered on Γ , or small hole pockets, centered at $\bar{S} = (\pi/2, \pi/2)$, and equivalent points. In dispersion studies, the hole pockets are associated with retrograde dispersion branches of low intensity (ghosts), particularly along $X \rightarrow S$ and $S \rightarrow \bar{S}$. Note that this negative curvature along the branch $X \rightarrow S$ is clearly seen for underdoped samples with $T_c \leq 75K$ ^{114,68}, Fig. 24. [Parenthetically, the striking difference in doping for the two data sets in this figure arises because Mar-

shall, et al.¹¹⁴ are plotting the normal state pseudogap, while Campuzano, et al.⁶⁸ plot the hump feature in the superconducting state.]

For these parameters, the transition to the paramagnetic phase is first order; for other parameter choices, a second-order transition is found. The first order transition is a topological transition, arising when the Fermi level crosses the band dispersion near X (Fig. 26). This is rather striking, since topological transitions are typically rather weak – of order 2.5. A similar result was found in the Hubbard model ($t' = 0$) by Guinea, et al.⁵⁶.

Thus, the dispersion of the normal state pseudogap, as seen in photoemission, can be well described by a uniform doping of the magnetic phase, in the absence of stripes. This has been noted by a number of groups, including Schmalian, et al.⁵⁴, and Misra, et al.⁵⁵. However, this cannot be the complete interpretation. Tunneling studies clearly demonstrate that the pseudogap consists of two components, split approximately symmetrically about the Fermi level. The uniform phase dispersion describes the feature *below* the Fermi level, but the model contains no corresponding feature above the Fermi level.

¹ J.M. Tranquada, B.J. Sternlieb, J.D. Axe, Y. Nakamura, and S. Uchida, Nature **375**, 561 (1995); J.M. Tranquada, J.D. Axe, N. Ichikawa, A.R. Moodenbaugh, Y. Nakamura, and S. Uchida, Phys. Rev. Lett. **78**, 338 (1997).

² K. Yamada, C.H. Lee, K. Kurahashi, J. Wada, S. Wakimoto, S. Ueki, H. Kimura, Y. Endoh, S. Hosoya, G. Shirane, R.J. Birgeneau, M. Greven, M.A. Kastner, and Y.J. Kim, Phys. Rev. B **57**, 6165 (1998).

³ T. Suzuki, T. Goto, K. Chiba, T. Shinoda, T. Fukase, H. Kimura, K. Yamada, M. Ohashi, and Y. Yamaguchi, Phys. Rev. B **57**, 3229 (1998); H. Kimura, K. Hirota, H. Matsushita, K. Yamada, Y. Endoh, S.-H. Lee, C.F. Majkrzak, R. Erwin, G. Shirane, M. Greven, Y.S. Lee, M.A. Kastner, and R.J. Birgeneau, Phys. Rev. B **59**, 6517 (1999).

⁴ S. Wakimoto, R.J. Birgeneau, Y. Endoh, P.M. Gehring, K. Hirota, M.A. Kastner, S.H. Lee, Y.S. Lee, G. Shirane, S. Ueki, and K. Yamada, cond-mat/9902201; S. Wakimoto, K. Yamada, S. Ueki, G. Shirane, Y. S. Lee, S. H. Lee, M. A. Kastner, K. Hirota, P. M. Gehring, Y. Endoh, R. J. Birgeneau, cond-mat/9902319.

⁵ Y.S. Lee, R.J. Birgeneau, M.A. Kastner, Y. Endoh, S. Wakimoto, K. Yamada, R.W. Erwin, S.H. Lee, and G. Shirane, cond-mat/9902157.

⁶ A.W. Hunt, P.M. Singer, K.R. Thurber, and T. Imai, cond-mat/9902348.

⁷ M.-H. Julien, F. Borsa, P. Carretta, M. Horvatić, C. Berthier, and C.T. Lin, Phys. Rev. Lett. **83**, 604 (1999).

⁸ P. Dai, H.A. Mook, and F. Dogan, Phys. Rev. Lett. **80**, 1738 (1998); H.A. Mook, P. Dai, S.M. Hayden, G. Aeppli, T.G. Perring, and F. Dogan, Nature **395**, 580 (1998).

⁹ M. Arai, T. Nishijima, Y. Endoh, T. Egami, S. Tajima,

- K. Tomimoto, Y. Shiohara, M. Takahashi, A. Garrett, and S.M. Bennington, Phys. Rev. Lett. **83**, 608 (1999).
- ¹⁰ A.V. Balatsky and P. Bourges, Phys. Rev. Lett. **82**, 5337 (1999).
- ¹¹ H.L. Edwards, A.L. Barr, J.T. Markert, and A.L. de Lozanne, Phys. Rev. Lett. **73**, 1154 (1994).
- ¹² H.A. Mook, F. Dogan, and B.C. Chakoumakos, Rome Conf. on Stripes, 1998 (to be published, J. Supercon.) (cond-mat/9811100).
- ¹³ R.J. McQueeney, T. Egami, Y. Petrov, M. Yethiraj, G. Shirane, and Y. Endoh, Bull. A.P.S. **43**, 964 (1998).
- ¹⁴ H.A. Mook, Miami Conf. on High-Temperature Superconductivity, 1999; M. Gutmann, S.J.L. Billinge, E.L. Brosha, and G.H. Kwei, cond-mat/9908365.
- ¹⁵ M. Akoshima, T. Noji, Y. Ono, and Y. Koike, Phys. Rev. **B57**, 7491 (1998).
- ¹⁶ N. Saini, J. Avila, A. Bianconi, A. Lanzara, M.C. Ascensio, S. Tajima, G.D. Gu, and N. Koshizuka, Phys. Rev. Lett. **79**, 3467 (1997).
- ¹⁷ Z.-X. Shen, P.J. White, D.L. Feng, C. Kim, G.D. Gu, H. Ikeda, R. Yoshizaki, and N. Koshizuka, Science **280**, 259 (1998).
- ¹⁸ J. Mesot, M. R. Norman, H. Ding, and J. C. Campuzano, cond-mat/9811027; J. C. Campuzano, H. Ding, H. Fretwell, J. Mesot, A. Kaminski, T. Yokoya, T. Takahashi, T. Mochiku, K. Kadowaki, cond-mat/9811349.
- ¹⁹ P.J. White, Z.-X. Shen, D.L. Feng, C. Kim, M.-Z. Hasan, J.M. Harris, A.G. Loeser, H. Ikeda, R. Yoshizaki, G.D. Gu, and N. Koshizuka, cond-mat/9901354.
- ²⁰ M.I. Salkola, V.J. Emery, and S.A. Kivelson, Phys. Rev. Lett. **77**, 155 (1996).
- ²¹ G. Seibold, F. Becca, F. Bucci, C. Castellani, C. di Castro, and M. Grilli, cond-mat/9906108.
- ²² D. Poilblanc and T.M. Rice, Phys. Rev. **B39**, 9749 (1989); H. Schulz, J. Phys. (Paris) **50**, 2833 (1989); J. Zaanen and O. Gunnarsson, Phys. Rev. **B40**, 7391 (1989); M. Inui and P.B. Littlewood, Phys. Rev. **B44**, 4415 (1991).
- ²³ J.A. Vergés, E. Louis, M.P. López-Sancho, F. Guinea, and A.R. Bishop, Phys. Rev. **B43**, 6099 (1991).
- ²⁴ K. Yonemitsu, A.R. Bishop, and J. Lorenzana, Phys. Rev. **B47**, 8065, 12059 (1993). cond-mat/9901164.
- ²⁵ B. Valenzuela, M. Vozmediano, and F. Guinea, cond-mat/9909224.
- ²⁶ G. Seibold, E. Sigmund, and V. Hizhnyakov, Phys. Rev. **B57**, 6937 (1998).
- ²⁷ For nickelates: S.H. Lee and S.-W. Cheong, Phys. Rev. Lett. **79**, 2514 (1997).
- ²⁸ S. Wakimoto, G. Shirane, Y. Endoh, K. Hirota, S. Ueki, K. Yamada, R.J. Birgeneau, M.A. Kastner, Y.S. Lee, P.M. Gehring, and S.H. Lee, Phys. Rev. **B60**, 769 (1999); S. Wakimoto, R.J. Birgeneau, M.A. Kastner, Y.S. Lee, R. Erwin, P.M. Gehring, S.H. Lee, M. Fujita, K. Yamada, Y. Endoh, K. Hirota, and G. Shirane, unpublished (cond-mat/9908115).
- ²⁹ C.H. Chen, S.-W. Cheong, and A.S. Cooper, Phys. Rev. Lett. **71**, 2461 (1993); S.-W. Cheong, H.Y. Hwang, C.H. Chen, B. Batlogg, L.W. Rupp, Jr., and S.A. Carter, Phys. Rev. **B49**, 7088 (1994).
- ³⁰ S. Mori, C.H. Chen, and S.-W. Cheong, Nature **392**, 473 (1998).
- ³¹ C.H. Chen, S.-W. Cheong, and A.S. Cooper, Phys. Rev. Lett. **71**, 2461 (1993); S.-W. Cheong, H.Y. Hwang, C.H. Chen, B. Batlogg, L.W. Rupp, Jr. and S.A. Carter, Phys. Rev. **B49**, 7088 (1994).
- ³² T. Muotu and H. Kontani, cond-mat/9904440.
- ³³ X.X. Bi and P.C. Ecklund, Phys. Rev. Lett. **70**, 2625 (1993).
- ³⁴ J. Zaanen and A.M. Oles, Ann. Physik **5**, 224 (1996).
- ³⁵ P.B. Visscher, Phys. Rev. **B10**, 943 (1974).
- ³⁶ E.L. Nagaev, "Physics of Magnetic Semiconductors" (Moscow, Mir, 1983).
- ³⁷ C. Nayak and F. Wilczek, Phys. Rev. Lett. **78**, 2465 (1997).
- ³⁸ V.J. Emery, and S.A. Kivelson, Physica **C209**, 597 (1993).
- ³⁹ A. Auerbach, and B.E. Larson, Phys. Rev. Lett. **66**, 2262 (1991).
- ⁴⁰ S.R. White and D.J. Scalapino, Phys. Rev. Lett. **80**, 1272 (1998).
- ⁴¹ S.R. White and D.J. Scalapino, Phys. Rev. Lett. **81**, 3227 (1998).
- ⁴² R. Hlubina, S. Sorella, and F. Guinea, Phys. Rev. Lett. **78**, 1343 (1997); R. Hlubina, Phys. Rev. **B59**, 9600 (1999).
- ⁴³ H.J. Schulz, Phys. Rev. **B39**, 2940 (1989).
- ⁴⁴ R.S. Markiewicz and M.T. Vaughn, J. Phys. Chem. Sol. **59**, 1737 (1998), and Phys. Rev. **B57**, 14052 (1998).
- ⁴⁵ R.S. Markiewicz, J. Phys. Cond. Matt. **2**, 665 (1990).
- ⁴⁶ R.S. Markiewicz, Phys. Rev. **B56**, 9091 (1997).
- ⁴⁷ H.-H. Lin, L. Balents, and M.P.A. Fisher, Phys. Rev. **B58**, 1794 (1998).
- ⁴⁸ R.S. Markiewicz, C. Kusko, and M.T. Vaughn, to be published, J. Supercond. (cond-mat/9807067).
- ⁴⁹ H. Tsunetsugu, M. Troyer, and T.M. Rice, Phys. Rev. **B51**, 16456 (1995).
- ⁵⁰ J.R. Schrieffer, X.G. Wen, and S.C. Zhang, Phys. Rev. **B39**, 11663 (1989).
- ⁵¹ A. Kampf and J. Schrieffer, Phys. Rev. **B41**, 6399 (1990).
- ⁵² N. Bulut, D.J. Scalapino, and S.R. White, Phys. Rev. Lett. **73**, 748 (1994).
- ⁵³ A.V. Chubukov and D.K. Morr, Phys. Rev. **B57**, 5298 (1998).
- ⁵⁴ J. Schmalian, D. Pines, and B. Stojković, Phys. Rev. Lett. **80**, 3839 (1998).
- ⁵⁵ S. Misra, R. Gatt, T. Schmauder, A.V. Chubukov, M. Onellion, M. Zacchigna, I. Vobornik, F. Zwick, M. Grioni, G. Margaritondo, C. Quitmann, and C. Kendziora, Phys. Rev. **B58**, 8905 (1998).
- ⁵⁶ F. Guinea, E. Louis, M.P. López-Sancho, and J.A. Vergés, cond-mat/9901164.
- ⁵⁷ B.O. Wells, Z.X. Shen, A. Matsuura, D.M. King, M.A. Kastner, M. Greven, and R.J. Birgeneau, Phys. Rev. Lett. **74**, 964 (1995).
- ⁵⁸ C. Kim, P.J. White, Z.-X. Shen, T. Tohyama, Y. Shibata, S. Maekawa, B.O. Wells, Y.J. Kim, R.J. Birgeneau, and M.A. Kastner, Phys. Rev. Lett. **80**, 4245 (1998); F. Ronning, C. Kim, D.L. Feng, D.S. Marshall, A.G. Loeser, L.L. Miller, J.N. Eckstein, I. Bozovic, and Z.-X. Shen, Science **282**, 2067 (1998).
- ⁵⁹ J.W. Loram, K.A. Mirza, J.R. Cooper, N.A. Thanasopoulou, and W.Y. Liang, in *Proceedings of the 10th Anniversary HTS Workshop on Physics, Materials, and Ap-*

- plications*, edited by B. Batlogg, C.W. Chu, D.U. Gubser, and K.A. Müller, (World Scientific, Singapore, 1996), p. 341; see discussion on pp. 1203-4 of Ref.⁶⁰.
- ⁶⁰ R.S. Markiewicz, *J. Phys. Chem. Sol.* **58**, 1179 (1997).
- ⁶¹ K. Dichtel, R.J. Jelitto, and H. Koppe, *Z. Physik*, **251**, 173 (1972).
- ⁶² H. Eskes and A.M. Oleś, *Phys. Rev. Lett.* **73**, 1279 (1994).
- ⁶³ S. Uchida, T. Ido, H. Takagi, T. Arima, Y. Tokura, and S. Tajima, *Phys. Rev. B* **43**, 7942 (1991).
- ⁶⁴ M. Veillette, Ya.B. Bazaliy, A.J. Berlinsky, and C. Kallin, *Phys. Rev. Lett.* **83**, 2413 (1999).
- ⁶⁵ J. Humlicek, A.P. Lityinchuk, W. Cress, B. Lederle, C. Thomsen, M. Cardona, H.L. Habermeier, I.E. Trofimov, and W. Konig, *Physica C* **206**, 345 (1993).
- ⁶⁶ A. Ino, C. Kim, M. Nakamura, T. Mizokawa, Z.-X. Shen, A. Fujimori, T. Kakeshita, H. Eisaki, and S. Uchida, *cond-mat/9902048*.
- ⁶⁷ R.B. Laughlin, *Phys. Rev. Lett.* **79**, 1726 (1997).
- ⁶⁸ J.C. Campuzano, H. Ding, M.R. Norman, H.M. Fretwell, M. Randeria, A. Kaminski, J. Mesot, T. Takeuchi, T. Sato, T. Yokoya, T. Takahashi, T. Mochiku, K. Kadowaki, P. Guptasarma, D.G. Hinks, Z. Konstantinovic, Z.Z. Li, and H. Raffy, *cond-mat/9906335*.
- ⁶⁹ J.F. Zasadzinski, *Bull. A.P.S.* **44**, 1503 (1999).
- ⁷⁰ A. Kaminski, J. Mesot, H. Fretwell, J.C. Campuzano, M.R. Norman, M. Randeria, H. Ding, T. Sato, T. Takahashi, T. Mochiku, K. Kadowaki, and H. Hoehst (*cond-mat/9904390*).
- ⁷¹ D.A. Bonn, P. Dosanjh, R. Liang, and W.L. Hardy, *Phys. Rev. Lett.* **68**, 2390 (1992); K. Krishana, J.M. Harris, and N.P. Ong, *Phys. Rev. Lett.* **75**, 3529 (1995); and M.R. Norman, M. Randeria, H. Ding, and J.C. Campuzano, *Phys. Rev. B* **57**, 11093 (1998).
- ⁷² R.S. Markiewicz, C. Kusko and V. Kidambi, *Phys. Rev. B* **60**, 627 (1999).
- ⁷³ A.V. Chubukov and D.K. Morr, *Phys. Rev. Lett.* **81**, 4716 (1998).
- ⁷⁴ Ar. Abanov and A.V. Chubukov, *Phys. Rev. Lett.* **83**, 1652 (1999).
- ⁷⁵ G. Aeppli, T.E. Mason, S.M. Hayden, H.A. Mook, and J. Culda, *Science* **278**, 1432 (1997).
- ⁷⁶ P. Carretta, T. Ciabattini, A. Cuccoli, E. Mognaschi, A. Rigamonti, V. Tognetti and P. Verrucchi, *cond-mat/9903450*.
- ⁷⁷ J. Schmalian, *cond-mat/9810041*.
- ⁷⁸ C. Castellani, C. Di Castro, and M. Grilli, *J. Phys. Chem. Solids*, *cond-mat/9804014*; S. Caprara, C. Castellani, C. Di Castro, M. Grilli, A. Perali, and M. Sulpizi, to be published, *J. Superconductivity*, *cond-mat/9812279*.
- ⁷⁹ G.S. Boebinger, Y. Ando, A. Passner, T. Kimura, M. Okuya, J. Shimoyama, K. Kishio, K. Tamasaku, N. Ichikawa, and S. Uchida, *Phys. Rev. Lett.* **77**, 5417 (1996).
- ⁸⁰ K. Segawa and Y. Ando, *cond-mat/9908124*.
- ⁸¹ R.B. Laughlin, *cond-mat/9709195*; J. Zaanen, *J. Phys. Chem. Solids* **59**, 1769 (1998).
- ⁸² P. Bourges, L.P. Regnault, J.Y. Henry, C. Vettier, Y. Sidis, and P. Burlet, *Physica B* **215**, 30 (1995).
- ⁸³ Y. Tokura, J.B. Torrance, T.C. Huang, and A.I. Nazzal, *Phys. Rev. B* **38**, 7156 (1988).
- ⁸⁴ J.L. Tallon, in "Proceedings of the 10th Anniversary HTS Workshop on Physics, Materials, an Applications," ed. by B. Batlogg, C.W. Chu, W.K. Chu, D.U. Gubser, and K.A. Müller, (World Scientific, Singapore, 1996), p. 292.
- ⁸⁵ J.L. Tallon, C. Bernhard, H. Shaked, R.L. Hitterman, and J.D. Jorgensen, *Phys. Rev. B* **51**, 12911 (1995).
- ⁸⁶ K. Yamada, S. Wakimoto, G. Shirane, C.H. Lee, M.A. Kastner, S. Hosoya, M. Greven, Y. Endoh, and R.J. Birgeneau, *Phys. Rev. Lett.* **75**, 1626 (1995); S. Petit, A.H. Moudden, B. Hennion, A. Vietkin, and A. Revcolevchi, *Physica B* **234-236**, 800 (1997).
- ⁸⁷ B. Lake, G. Aeppli, T.E. Mason, A. Schröder, D.F. McMorrow, K. Lefmann, M. Isshiki, M. Nohara, H. Takagi, and S.M. Hayden, *Nature* **400**, 43 (1999).
- ⁸⁸ E. Dagotto and T.M. Rice, *Science* **271**, 618 (1996).
- ⁸⁹ S. Gopalan, T.M. Rice, and M. Sigrist, *Phys. Rev. B* **49**, 8901 (1994).
- ⁹⁰ P. Bourges, in "Gap Symmetry and Fluctuations in High Temperature Superconductors," ed. by J. Bok, G. Deutscher, D. Pavuna, and S.A. Wolf (Plenum, NY, 1998).
- ⁹¹ L.P. Regnault, I. Zaliznyak, J.P. Renard, and C. Vettier, *Phys. Rev. B* **50**, 9174 (1994).
- ⁹² Y.-J. Kim, R.J. Birgeneau, M.A. Kastner, Y.S. Lee, Y. Endoh, G. Shirane, and K. Yamada, *cond-mat/9902248*.
- ⁹³ T. Sato, T. Yokoya, Y. Naitoh, T. Takahashi, K. Yamada, and Y. Endoh, *Phys. Rev. Lett.* **83**, 2254 (1999).
- ⁹⁴ A. Bianconi, A. Valletta, A. Perali, and N.L. Saini, *Physica C* **296**, 269 (1998); C.C. Tsuei and T. Doderer, *Eur. Phys. J B* **10**, 257 (1999).
- ⁹⁵ N. Miyakawa, J.F. Zasadzinski, L. Ozyuzer, P. Guptasarma, D.G. Hinks, C. Kendziora, and K.E. Gray, *Phys. Rev. Lett.* **83**, 1018 (1999).
- ⁹⁶ R.S. Markiewicz and C. Kusko, *cond-mat/9810214*.
- ⁹⁷ D.L. Feng, W.J. Zheng, K.M. Shen, D.H. Lu, F. Ronning, J.-I. Shimoyama, K. Kishio, G. Gu, D. Van der Marel, and Z.-X. Shen, *cond-mat/9908056*.
- ⁹⁸ H.M. Fretwell, A. Kaminski, J. Mesot, J.C. Campuzano, M.R. Norman, M. Randeria, T. Sato, R. Gatt, T. Takahashi, and K. Kadowaki, *cond-mat/9910221*; J. Mesot, A. Kaminski, H.M. Fretwell, M. Randeria, J.C. Campuzano, H. Ding, M.R. Norman, T. Takeuchi, T. Sato, T. Yokoya, T. Takahashi, I. Chong, T. Terashima, M. Takano, T. Mochiku, and K. Kadowaki, *cond-mat/9910430*.
- ⁹⁹ P. Blakeslee, R.J. Birgeneau, F.C. Chou, R. Christianson, M.A. Kastner, Y.S. Lee, and B.O. Wells, *Phys. Rev. B* **57**, 13915 (1998).
- ¹⁰⁰ R.B. Laughlin, *J. Phys. Chem. Sol.* **56**, 1627 (1995).
- ¹⁰¹ X.-G. Wen and P.A. Lee, *Phys. Rev. Lett.* **76**, 503 (1996).
- ¹⁰² L.P. Pryadko, S.A. Kivelson, V.J. Emery, Y.B. Bazaliy, and E.A. Demler, *cond-mat/9905146*.
- ¹⁰³ J.P. Lu, Q. Si, J.H. Kim, and K. Levin, *Physica C* **179**, 191 (1991).
- ¹⁰⁴ This can most clearly be seen from Fig. 2 of Y.-J. Kao, Q. Si, and K. Levin, *cond-mat/9908302*. Note that in this model the parts of the Fermi surface nearest the VHS contribute weight *away* from the incommensurate peaks.
- ¹⁰⁵ B. Stojković and D. Pines, *Phys. Rev. Lett.* **76**, 811 (1996).
- ¹⁰⁶ W.O. Putikka, R.L. Glenister, and R.R.P. Singh, *Phys. Rev. Lett.* **73**, 170 (1994); C.T. Shih, Y.C. Chen, and T.K. Lee, *Phys. Rev. B* **57**, 627 (1998); and M. Calandra,

- F. Becca, and S. Sorella, Phys. Rev. Lett. **81**, 5185 (1998).
- ¹⁰⁷ C.S. Hellberg and E. Manousakis, Phys. Rev. Lett. **83**, 132 (1999).
- ¹⁰⁸ S.R. White and D.J. Scalapino, unpublished (cond-mat/9907243 and cond-mat/9907375).
- ¹⁰⁹ C.S. Hellberg and E. Manousakis, unpublished (cond-mat/9910142).
- ¹¹⁰ L. P. Pryadko, S. Kivelson and D. W. Hone, Phys. Rev. Lett, **80**, 5651 (1998).
- ¹¹¹ T. Tohyama, C. Gazza, C.T. Shih, Y.C. Chen, T.K. Lee, S. Maekawa, and E. Dagotto, cond-mat/9809411.
- ¹¹² S.R. White and D.J. Scalapino, Phys. Rev. **B60**, 753 (1999).
- ¹¹³ R.S. Markiewicz and M.T. Vaughn, in “High Temperature Superconductivity”, ed. by S.E. Barnes, J. Ashkenazi, J.L. Cohn, and F. Zuo (AIP, Woodbury, NY, 1999), p. 75.
- ¹¹⁴ D.S. Marshall, D.S. Dessau, A.G. Loeser, C.-H. Park, A.Y. Matsuura, J.N. Eckstein, I. Bozovic, P. Fournier, A. Kapitulnik, W.E. Spicer, and Z.-X. Shen, Phys. Rev. Lett. **76**, 4841 (1996).
- ¹¹⁵ C. Kusko and R.S. Markiewicz, cond-mat/9903317.